



Quantitative  
evaluation of ozone  
and selected climate  
parameters in EMAC

M. Righi et al.

# Quantitative evaluation of ozone and selected climate parameters in a set of EMAC simulations

M. Righi<sup>1</sup>, V. Eyring<sup>1</sup>, K.-D. Gottschaldt<sup>1</sup>, C. Klinger<sup>1,\*</sup>, F. Frank<sup>1</sup>, P. Jöckel<sup>1</sup>, and I. Cionni<sup>2</sup>

<sup>1</sup>Deutsches Zentrum für Luft- und Raumfahrt (DLR), Institut für Physik der Atmosphäre, Oberpfaffenhofen, Germany

<sup>2</sup>Agenzia nazionale per le nuove tecnologie, l'energia e lo sviluppo economico sostenibile (ENEA), Rome, Italy

\*now at: Ludwig-Maximilians-Universität München, Fakultät für Physik, Meteorologisches Institut, Munich, Germany

Received: 22 July 2014 – Accepted: 13 August 2014 – Published: 2 October 2014

Correspondence to: M. Righi (mattia.righi@dlr.de)

Published by Copernicus Publications on behalf of the European Geosciences Union.

Title Page

Abstract

Introduction

Conclusions

References

Tables

Figures



Back

Close

Full Screen / Esc

Printer-friendly Version

Interactive Discussion



## Abstract

Four simulations with the ECHAM/MESy Atmospheric Chemistry (EMAC) model have been evaluated with the Earth System Model Validation Tool (ESMValTool) to identify differences in simulated ozone and selected climate parameters that resulted from (i) different setups of the EMAC model (nudged vs. free-running) and (ii) different boundary conditions (emissions, sea surface temperatures (SSTs) and sea-ice concentrations (SICs)). To assess the relative performance of the simulations, quantitative performance metrics are calculated consistently for the climate parameters and ozone. This is important for the interpretation of the evaluation results since biases in climate can impact on biases in chemistry and vice versa. The observational datasets used for the evaluation include ozonesonde and aircraft data, meteorological reanalyses and satellite measurements. The results from a previous EMAC evaluation of a model simulation with weak nudging towards realistic meteorology in the troposphere have been compared to new simulations with different model setups and updated emission datasets in free-running timeslice and nudged Quasi Chemistry-Transport Model (QCTM) mode. The latter two configurations are particularly important for chemistry-climate projections and for the quantification of individual sources (e.g. transport sector) that lead to small chemical perturbations of the climate system, respectively. With the exception of some specific features which are detailed in this study, no large differences that could be related to the different setups of the EMAC simulations (nudged vs. free-running) were found, which offers the possibility to evaluate and improve the overall model with the help of shorter nudged simulations. The main differences between the two setups is a better representation of the tropospheric and stratospheric temperature in the nudged simulations, which also better reproduce stratospheric water vapour concentrations, due to the improved simulation of the temperature in the tropical tropopause layer. Ozone and ozone precursor concentrations on the other hand are very similar in the different model setups, if similar boundary conditions are used. Different boundary conditions however lead to relevant differences in the four simulations. SSTs and

GMDD

7, 6549–6627, 2014

### Quantitative evaluation of ozone and selected climate parameters in EMAC

M. Righi et al.

Title Page

Abstract

Introduction

Conclusions

References

Tables

Figures



Back

Close

Full Screen / Esc

Printer-friendly Version

Interactive Discussion

















a 10 year climatology from 1995 to 2004. The emission setup is the same as in the the QCTM experiment, but it considers only the year 2000.

### 3.4 Simulation in free-running mode: ACCMIP

This timeslice simulation was performed in support of the Atmospheric Chemistry and Climate Model Intercomparison Project (ACCMIP; Lamarque et al., 2013). The simulation is identical to the TS2000 setup, except that slightly different emission inventories were used (see Table S1), in order to conform to the project requirements. This timeslice simulation is only one out of the ACCMIP series of experiments, covering the period 1850 to 2100. The corresponding EMAC simulations are evaluated and analyzed in a variety of ACCMIP papers (Fiore et al., 2012; Naik et al., 2013; Silva et al., 2013; Stevenson et al., 2013; Voulgarakis et al., 2013; Young et al., 2013). To allow a consistent use of SSTs/SICs that cover the full period without discontinuities, simulated SSTs/SICs from a long-term climate model simulation were prescribed instead of using observations as in TS2000. Monthly mean SSTs and SICs are prescribed as a 10 year climatological mean around the base year 2000 using the historical CMIP5 experiment carried out with the Centro Euro-Mediterraneo sui Cambiamenti Climatici (CMCC) climate model, which is based on ECHAM5 like EMAC. A comparison of the CMCC SSTs to the climatology from the HAdIIST data for the same period shows significant differences (up to  $\sim 2$  K) over large areas of the ocean (Fig. S1). Note that because of the too short period, this is not an evaluation of the CMCC SSTs/SICs but rather just documents the differences between the two datasets that are prescribed in the TS2000 and ACCMIP simulations.

## 4 Diagnostics, performance metrics and evaluation tool

In order to quantitatively assess and compare the ability of the different EMAC simulations in representing key features of observed climate and chemical composition, basic

GMDD

7, 6549–6627, 2014

### Quantitative evaluation of ozone and selected climate parameters in EMAC

M. Righi et al.

Title Page

Abstract

Introduction

Conclusions

References

Tables

Figures

⏪

⏩

◀

▶

Back

Close

Full Screen / Esc

Printer-friendly Version

Interactive Discussion



## Quantitative evaluation of ozone and selected climate parameters in EMAC

M. Righi et al.

Title Page

Abstract

Introduction

Conclusions

References

Tables

Figures



Back

Close

Full Screen / Esc

Printer-friendly Version

Interactive Discussion



statistical measures are calculated in addition to the diagnostic plots that provide more detailed insights. For each diagnostic, the root mean square difference (RMSD), the overall mean bias, and the Taylor diagram are presented. The RMSD and bias metrics are calculated considering the space–time field (latitude, longitude plus annual cycle) where available, or only the annual cycle otherwise.

Following Gleckler et al. (2008), the RMSD and overall mean bias in the annual cycle of different mean climate parameters at a particular pressure level is calculated within four different domains (global, tropics, NH extratropics and SH extratropics). The results of such quantitative evaluation are presented as portrait diagrams, where the RMSD gives positive values only (due to squaring), whereas the overall mean bias is also sensitive to the sign of the deviation, being positive (negative) when the model overestimates (underestimates) the observations. To compare the relative performance of the simulations, the RMSD and bias are normalized by dividing through their multi-model average (see Appendices A1 and A2 for details).

All diagnostics and performance metrics shown in this paper have been implemented into the Earth System Model Validation Tool (ESMValTool), which is an extension of the previously-developed CCMVal Diagnostic Tool for chemistry-climate models (Gettelman et al., 2012) to Earth System Models (ESMs). This ensures that the analysis presented in this paper can be applied to other EMAC simulations and other ESMs in a routine manner.

The ESMValTool is designed to work on model output formatted according to the Climate Model Output Rewriter (CMOR) standard (see <http://www2-pcmdi.llnl.gov/cmor>). The CMOR standard defines, for example, standard names for variables, units, coordinates names and values, etc. A reformatting routine is implemented in the ESMValTool that converts the original EMAC model output to the format required for the tool. Applying this reformatting routine to new EMAC simulations is straightforward, so that new simulations can be easily compared to the results shown here. The reformatting routine can also serve as an example for converting the output of other ESMs.

The ESMValTool is developed as an international community tool by multiple institutions with the goal to enhance routine benchmarking and evaluation of ESMs. The priority of the effort so far has been to target specific scientific themes focusing on selected Essential Climate Variables (ECVs), tropical variability (e.g. Monsoon), Southern ocean, continental dry bias and soil hydrology-climate interactions, carbon dioxide (CO<sub>2</sub>), aerosols and ozone, but the package is being developed in such a way that additional analysis can be easily added. In this way the standard for model evaluation can be built up over time. For further information and updates, see the ESMValTool website at <http://www.pa.op.dlr.de/ESMValTool>.

## 5 Observational data for model evaluation

A variety of different observations are used for the model evaluation. For most variables, we choose a reference and an alternative dataset in order to estimate differences and uncertainties in observations.

A summary of the main diagnostics applied in this study is given in Table 3, along with the variables, observations, the short names and period/domain for the performance metrics and corresponding references.

### 5.1 Temperature, winds, geopotential height and specific humidity

For global temperature, winds, geopotential height and specific humidity, meteorological reanalyses are the best available reference data. Reanalysis projects provide spatially complete and coherent records of atmospheric variables. Given the improvement of models, input data and assimilation methods, reanalyses have significantly improved in reliability, cover longer time-periods and have increased in spatial and temporal resolution (Dee et al., 2011).

We use two different reanalysis datasets (ERA-Interim and NCEP/NCAR, see below) for the comparisons to simulated temperature, wind, geopotential height and specific

GMDD

7, 6549–6627, 2014

## Quantitative evaluation of ozone and selected climate parameters in EMAC

M. Righi et al.

Title Page

Abstract

Introduction

Conclusions

References

Tables

Figures

◀

▶

◀

▶

Back

Close

Full Screen / Esc

Printer-friendly Version

Interactive Discussion



## Quantitative evaluation of ozone and selected climate parameters in EMAC

M. Righi et al.

Title Page

Abstract

Introduction

Conclusions

References

Tables

Figures

◀

▶

◀

▶

Back

Close

Full Screen / Esc

Printer-friendly Version

Interactive Discussion



humidity. The differences between the climatologies derived from these fields are an indicator of the uncertainties in the meteorological analyses. ERA-Interim reanalysis is produced by the ECMWF and covers the period from 1979 to present (Dee et al., 2011). All observations used in the reanalysis undergo quality control, selection steps (e.g. to sort out duplicate reports or data that is known to have large errors) and bias corrections (Dee et al., 2011). We therefore consider ERA-Interim as the main reference dataset for meteorological fields in this work and analyse the period 1995–2005.

In addition, the NCEP/NCAR reanalysis is applied, which covers the period from 1948 to present (Kalnay et al., 1996). Over the reanalysis period, developments in the observation system took place, particularly when satellite observations became available in the 1970s. Consistently with ERA-Interim, we analyse the period 1995–2005.

For specific humidity, we follow Gleckler et al. (2008) and use observations from the Atmospheric Infrared Sounder (AIRS) experiment (Aumann et al., 2003) as our reference data set and ERA-Interim as alternative. AIRS data are available from the middle of 2002 to the middle of 2011. The data used in this work cover the years 2003 to 2010.

Vertical and meridional profiles of climatological zonal mean water vapour volume mixing ratios are compared to measurements taken by the HALogen Occultation Experiment (HALOE) on board of the Upper Atmosphere Research Satellite (UARS), launched in 1991 (Russell et al., 1993). Model climatologies are formed for the period 1991–2002 (Groß and Russell III, 2005). HALOE data for H<sub>2</sub>O ranges from about 11 to 65 km altitude and cover 80° S to 80° N in latitude within one year. For all measured species the accuracy of the HALOE retrievals decreases near the tropopause (Brühl et al., 1996; Harries et al., 1996; Park et al., 1996; Russell et al., 1996) and sparse coverage of the polar regions increases the uncertainty in the HALOE climatologies there.

## 5.2 Radiation

For evaluating radiation fluxes, our primary dataset is taken from the Surface Radiation Budget Project (SRB; GEWEX-news, 2011) and the alternative dataset is taken from the Clouds and the Earth's Radiant Energy System (CERES; Wielicki et al., 1996) experiment. The SRB dataset in its current version (3.0) covers the period from July 1983 to December 2007. Here we consider the time range 1995–2005. The dataset provides surface and top of the atmosphere (ToA) longwave and shortwave fluxes derived from a variety of satellite-observed parameters, like cloud parameters, ozone fields and re-analysis meteorology (GEWEX-news, 2011). The CERES experiment products include information about solar and longwave radiation for the surface and ToA between 2001 and 2005.

## 5.3 Total column ozone

For the evaluation of total column ozone, we use the NIWA combined total column ozone dataset over the period 1998–2010 as reference dataset (Bodeker et al., 2005) and a combined dataset from the Global Ozone Monitoring Experiment (GOME) and GOME-2 for the same period as alternative (Loyola and Coldewey-Egbers, 2012; Loyola et al., 2009). The NIWA dataset is an assimilated database that combines TOMS (Total Ozone Mapping Spectrometer), GOME and SBUV (Solar Backscatter Ultra-Violet radiometer) data. In order to obtain a global homogeneous dataset, ground-based data from the Dobson spectrophotometer network are used, removing differences between the individual input data or filling existing gaps.

## 5.4 Tropospheric ozone

For the evaluation of tropospheric column ozone we use a global climatology based on the Aura Ozone Monitoring Instrument (OMI) and Microwave Limb Sounder (MLS) ozone measurements for the period 2005–2012 (Ziemke et al., 2006, 2011). The

# GMDD

7, 6549–6627, 2014

## Quantitative evaluation of ozone and selected climate parameters in EMAC

M. Righi et al.

Title Page

Abstract

Introduction

Conclusions

References

Tables

Figures



Back

Close

Full Screen / Esc

Printer-friendly Version

Interactive Discussion



MLS/OMI gridded ozone climatology data are made available to the scientific community via the NASA Goddard Space Flight Center ozone and air quality website (<http://ozoneaq.gsfc.nasa.gov/>).

For the comparison of ozone vertical profiles in the troposphere, we use a recently updated global climatology by Tilmes et al. (2012), based on ozone soundings over the last 15 years and focusing on the troposphere and the lower stratosphere. This is an important extension to the Logan (1999) climatology, since it covers the more recent years included in the simulated period of the experiments evaluated here. Vertical ozone profiles for 41 stations around the globe have been compiled and averaged for the years 1980–2009. The climatology provides information about the median and the width of the ozone probability distribution function, as well as the interannual variability of ozone between 1995 and 2009, in pressure- and tropopause-referenced altitudes. In addition to single stations, regional aggregates are included, combining stations with similar ozone characteristics. We use these regional aggregates for model evaluation and focus on the 1995–2009 time period, corresponding to the simulated period of our experiments.

In addition, we use ozone data from a collection of aircraft campaigns (Emmons et al., 2000). These data are particularly valuable because they include additional species, measured at the same location and time of ozone, allowing a more detailed analysis on ozone precursor species. These data are provided as global distribution and vertical profiles and were validated against ozonesondes and measurements on-board commercial aircraft. The ozone data cover only selected regions of the Earth and time periods vary for each region.

## 5.5 Ozone precursors

For the evaluation of ozone precursors, we use again the Emmons et al. (2000) dataset, which provides information about a variety of species, including CH<sub>4</sub>, CO, NO<sub>x</sub> and NMHCs.

## Quantitative evaluation of ozone and selected climate parameters in EMAC

M. Righi et al.

Title Page

Abstract

Introduction

Conclusions

References

Tables

Figures

◀

▶

◀

▶

Back

Close

Full Screen / Esc

Printer-friendly Version

Interactive Discussion



**Quantitative  
evaluation of ozone  
and selected climate  
parameters in EMAC**

M. Righi et al.

[Title Page](#)[Abstract](#)[Introduction](#)[Conclusions](#)[References](#)[Tables](#)[Figures](#)[Back](#)[Close](#)[Full Screen / Esc](#)[Printer-friendly Version](#)[Interactive Discussion](#)

For the evaluation of CO, we additionally use the observational data from the NOAA GLOBALVIEW dataset (4th annual update, GLOBALVIEW-CO<sub>2</sub>, 2010), over the 1998–2008 period. This dataset is provided by the Cooperative Atmospheric Data Integration Project for Carbon Monoxide which is coordinated by NOAA (National Oceanic and Atmospheric Administration), ESRL (Earth System Research Laboratory) and GMD (Global Monitoring Division). The goal of the GLOBALVIEW initiative was to get data products with a large spatial and temporal resolution to support carbon cycle modelling studies based on measurements from land-surface, ship, aircraft, and tower observations. The processing includes smoothing, interpolation and extrapolation following Masarie and Tans (1995), resulting in an extended record.

## 6 Results and discussion of model evaluation

### 6.1 Basic climate parameters

In the following subsections, we first evaluate how well the mean climate state in selected basic climate variables such as temperature, eastward and northward wind, geopotential height, specific humidity and radiation is represented in the four simulations. In the choice of the tropospheric diagnostics and performance metrics we closely follow those that were applied by Gleckler et al. (2008), with periods changed to represent 2000 conditions. Since the EVAL2 and the QCTM simulations are both nudged by meteorological reanalysis, a generally better agreement with meteorological reanalyses compared to the free-running timeslice experiments (TS2000 and ACCMIP) can be expected. However, since the nudging is relatively weak, differences could still occur, in particular in regions where the nudging parameters are small, i.e. outside the main nudging interval, which is between  $\sim 97$  hPa and  $\sim 706$  hPa (see Sect. 3.1).

## 6.1.1 Temperature

Temperature ( $t_a$ ) is evaluated by investigating the climatological mean annual cycle at the four selected pressure levels 850, 200, 300 and 5 hPa (Fig. 1) and the annual mean zonally averaged temperature differences between each EMAC simulations and the reference data set (ERA-Interim, Fig. 2) and the alternative dataset (NCEP).

The annual cycle is in general well reproduced by all simulations at all levels and in all regions, with the exception of the 200 hPa level in the tropics. At 850 hPa, all EMAC simulations are in good agreement with ERA-Interim and NCEP/NCAR and lie generally within the interannual variability of the meteorological reanalyses, with the exception of ACCMIP which shows a positive bias ( $\sim 1$  K) in the tropical NH summer months (JJA). Such overestimation can be explained by the positive bias of the tropical SSTs in the prescribed dataset (see Fig. S1), which for the ACCMIP simulation is taken from a historical simulation with the CMCC climate model (see Sect. 3.4). Both the meteorological reanalyses and the model simulations are characterized by a very small interannual variability at this level (Fig. 1).

At 200 hPa, all EMAC simulations have a cold bias of around 5 K in all regions compared to the meteorological reanalyses and are well outside the interannual variability. This bias is particularly pronounced in the tropics in the two nudged simulations, whereas in the extratropics of both hemispheres the nudged simulations are in slightly better agreement with ERA-Interim than the free-running timeslice simulations.

Stratospheric temperatures at 30 and 5 hPa (Fig. 1, lower rows) are within one standard deviation of ERA-Interim in the extratropics in all simulations, with the exception of the summer months in NH. In the tropics, a cold bias of around 2 K is simulated. At 5 hPa in the tropics, ACCMIP and TS2000 show a better agreement with the observations than the other experiments. In general, temperature is much better simulated in the lower troposphere, where the simulated deviations from ERA-Interim are of similar magnitude than the differences between the two reanalysis datasets, which are anyway small and suggest therefore low uncertainties in the reference and alternative dataset.

# GMDD

7, 6549–6627, 2014

## Quantitative evaluation of ozone and selected climate parameters in EMAC

M. Righi et al.

Title Page

Abstract

Introduction

Conclusions

References

Tables

Figures



Back

Close

Full Screen / Esc

Printer-friendly Version

Interactive Discussion









The other simulations reproduce the annual cycle quite well and are within the interannual variability of the observations. In the extratropics, a small negative bias is found in winter for all simulations, in particular at 30 hPa.

Figures 8 and S4 show the difference plots of the seasonal mean of the eastward wind in DJF and JJA, respectively. A generally good agreement between the EMAC simulations and ERA-Interim is simulated, and especially the summertime stratospheric easterlies are well represented in all simulations. Some weaknesses are found however in the simulations of westerlies. In DJF (Fig. 8), the subtropical jet is underestimated at about 60° S in the free-running simulations (TS2000 and ACCMIP), while the nudged simulations capture the jet. On the other hand, the nudged simulations underestimate the polar night jet in the northern polar regions. Such underestimation might be related to a weak representation of the polar vortex in the NH. The temperature profiles for DJF (not shown) for the nudged simulations show indeed a warm bias in this specific region, which might be an indication for a too weak polar vortex. In JJA (Fig. S4), the westwind jet at 60° S is severely underestimated by the free-running simulations throughout the entire atmosphere, while the nudged simulations underestimate westerlies in the stratosphere. The underestimation of the west wind jets in the free-running simulations reveal a too weak polar vortex. As shown in Sect. 6.1.1, the seasonal mean of the temperature (Fig. S2) showed a warm bias in this region. Both, the weaker winds and the higher temperatures are an indication of an underestimation of the polar vortex.

The better performance of the nudged simulations with respect to the free-running simulations in the lower troposphere (850 hPa) is revealed by the portrait diagrams (Figs. 5 and 6). The eastward wind is generally underestimated in the extratropics and in the global domain, whereas it is overestimated in the tropics, especially in the stratosphere. As for the temperature, there are differences in the model performance with respect to the two meteorological reanalyses considered for the evaluation, which reveals potential uncertainties in the observational datasets. These considerations are further supported by the Taylor diagram (Fig. 7), which shows an excellent representation of

## GMDD

7, 6549–6627, 2014

### Quantitative evaluation of ozone and selected climate parameters in EMAC

M. Righi et al.

Title Page

Abstract

Introduction

Conclusions

References

Tables

Figures



Back

Close

Full Screen / Esc

Printer-friendly Version

Interactive Discussion



the eastward wind globally and in the extratropics by all model simulations. In the tropical domain, on the other hand, variations in the phase and amplitude are significantly larger.

### 6.1.3 Northward wind, geopotential height and specific humidity

Northward wind, geopotential height and specific humidity are evaluated mainly to assess whether there are some serious limitations in the simulation of the mean and only discussed briefly.

The northward wind ( $v_a$ ) at the four selected levels (850, 200, 30, and 5 hPa) mostly lies within the interannual variability of the ERA-Interim reanalysis, with differences between ERA-Interim and NCEP being in the same order or larger than differences to the model simulations (Fig. S5). The annual mean zonally averaged plot (Fig. S6) show that, in general, the major features are well reproduced by all model setups. The portrait diagrams (Figs. 5 and 6) further confirm the expected generally better performance of the nudged simulations compared to the free running ones. In the overall mean bias diagram, northward winds are found to be either overestimated or underestimated depending on the considered observational datasets.

The comparison of simulated geopotential height ( $z_g$ ) with observations shows a generally good agreement (see Figs. S7 and S8), with relative differences of the order of a few percent. The annual cycle is mostly captured. Differences of the same order, however, can also be found when comparing ERA-Interim with NCEP data, revealing some uncertainties in the meteorological reanalyses as well.

The annual cycle of the specific humidity ( $hus$ ) is mostly captured by the EMAC simulations (Fig. S9), with the exception of the tropical domain, in particular at the 30 hPa level. Following Gleckler et al. (2008), instead of the 200 hPa level we consider 400 hPa, since this is more significant for the evaluation of specific humidity in the troposphere. In the extratropics, the annual cycle shows a clear maximum in the summer months, following the change in incoming solar radiation during the year which affects water evaporation. In the tropics, on the other hand, the annual cycle shows a much smaller

**Quantitative  
evaluation of ozone  
and selected climate  
parameters in EMAC**

M. Righi et al.

Title Page

Abstract

Introduction

Conclusions

References

Tables

Figures



Back

Close

Full Screen / Esc

Printer-friendly Version

Interactive Discussion



variation with time, since in this region the change in incoming radiation during the year is much less pronounced. The nudged simulations, which are driven by ECMWF operational analysis data, are generally closer to ERA-Interim than to AIRS data, while the free-running simulations simulate monthly mean values closer to the AIRS data in the lower troposphere. The general pattern of the specific humidity profile climatology (Fig. S10) is characterized by a maximum over the equator at the surface, decreasing with latitude and altitude, and is well reproduced by all simulations.

#### 6.1.4 Radiation

Climatological mean maps of outgoing longwave clear-sky radiation at the ToA (rlutcs) are shown in Fig. S11, compared with SRB and CERES. The observational data (Fig. S11, upper row, left) displays its highest values in the tropics (about  $300 \text{ W m}^{-2}$ ) and two clear minima over the poles (around  $150 \text{ W m}^{-2}$  at the South and  $200 \text{ W m}^{-2}$  at the North). The EMAC simulations capture these features as can be seen in the differences plots (Fig. S11). Compared to SRB, variations smaller than  $20 \text{ W m}^{-2}$  are found everywhere on the globe, with a clear overestimation over the South polar regions (about  $10 \text{ W m}^{-2}$ , 5–10%), which is stronger in the free-running simulations. The other parts of the globe show a general underestimation (maximum biases of about  $30 \text{ W m}^{-2}$ , 10–20%) which is stronger in the nudged simulations. A similar difference pattern results from the comparison between EMAC and CERES.

The outgoing longwave all-sky radiation at the ToA (rlut) is compared again to SRB and CERES (Fig. S12). The observations show a maximum value over the tropics ( $250\text{--}300 \text{ W m}^{-2}$ ) and two extended minima over the polar regions (about  $150 \text{ W m}^{-2}$  for the South and  $200 \text{ W m}^{-2}$  for the North). In general, the radiation values are lower than for clear-sky conditions (Fig. S11), as expected due to the presence of clouds. All EMAC simulations show a similar pattern of deviations compared to SRB, with the free-running experiments characterized by the largest differences (about  $20\text{--}30 \text{ W m}^{-2}$ ). Biases of about  $10\text{--}20 \text{ W m}^{-2}$  in the tropics were also found for the CMIP3 models when

Title Page

Abstract

Introduction

Conclusions

References

Tables

Figures



Back

Close

Full Screen / Esc

Printer-friendly Version

Interactive Discussion



compared to ERBE data (IPCC, 2007), although some had very large deviations (up to about  $50 \text{ W m}^{-2}$ ).

Another important quantity for the evaluation of the radiation budget is the reflected shortwave all-sky radiation ( $r_{\text{sut}}$ , Fig. S13). The net shortwave radiation is primarily determined by solar incoming radiation and by the presence of clouds. The general pattern is therefore a combination of the variation of incoming solar radiation with latitude/season and of cloud cover. The EMAC simulations reproduce this pattern well (Fig. S13). The observations show their highest values (around  $120\text{--}150 \text{ W m}^{-2}$ ) over regions of high surface albedo or significant cloud cover (deserts, snow covered areas, Himalaya and Sahara), while the strongly absorbing ocean surface is characterized by lower values ( $60\text{--}80 \text{ W m}^{-2}$ ). The comparison of EMAC simulations with SRB and CERES data shows a positive bias at mid-latitudes and in polar regions, with the highest deviations ( $30\text{--}40 \text{ W m}^{-2}$ ,  $10\text{--}20\%$ ) in northern higher latitudes (Alaska, North-East Russia), which are particularly present in the EVAL2 simulation. Negative biases are found in the tropics and subtropics, up to about  $20\text{--}30 \text{ W m}^{-2}$  ( $20\text{--}30\%$ ) in the ITCZ. This pattern is consistent with the general tendency of EMAC to underestimate low cloud fraction in the tropics and to overestimate it in the extratropics in comparison with ISCCP satellite data (Räisänen and Järvinen, 2010). These results are summarized in the performance metrics plots (Figs. 5 and 6).

## 6.2 Ozone and ozone precursors

In this paper we focus on tropospheric ozone, and consider the stratosphere only in the context of total column ozone. Biases in tropospheric ozone found in all four EMAC simulations led to two additional simulations (ACCMIP-S1 and ACCMIP-S2) to explore related model uncertainties. These two simulations are included in the figures, but discussed separately in Sect. 6.2.5.

# GMDD

7, 6549–6627, 2014

## Quantitative evaluation of ozone and selected climate parameters in EMAC

M. Righi et al.

Title Page

Abstract

Introduction

Conclusions

References

Tables

Figures

⏪

⏩

◀

▶

Back

Close

Full Screen / Esc

Printer-friendly Version

Interactive Discussion



## 6.2.1 Total column ozone

Zonal mean total column ozone (toz) climatologies from the different EMAC simulations are compared to the NIWA assimilated data and observations from the GOME instrument in Figs. 9 and 10. The well-known features of highest column ozone values in NH spring, low ozone values in the tropics, with a small seasonal cycle, a column-ozone maximum in the mid-latitudes of the SH in late winter/early spring and the ozone hole above the Antarctic are well represented the EMAC simulations, but significant quantitative differences compared to observations do exist. The ozone hole is underestimated in all EMAC simulations, in particular in TS2000, where the ozone hole is only marginally present and underestimated by around 75–100 DU. In NH winter, EMAC simulations overestimate column ozone in the high latitudes by around 100 DU compared to NIWA observations, but differences of about 50 DU also exist between the two observational datasets, with GOME showing higher values in this region. At about 50–60° S, the mid-latitude maximum in total column ozone in autumn is produced by all EMAC simulations, but is more pronounced than in the NIWA and GOME observations. In the tropics the EMAC simulations show good agreement with NIWA and GOME observations. The above features are also reflected in the zonal mean total ozone values for the different seasons and the annual mean (Fig. 10).

The main difference between the two free-running simulations, TS2000 and ACCMIP, is in the prescribed SSTs. A key impact of SSTs on stratospheric ozone is attributed to differences in the meridional circulation and the underlying wave forcing. The SST signal propagates to the stratosphere by modulation of the planetary wave activity and thus the Brewer–Dobson-Circulation (Garny et al., 2009). Compared to ACCMIP, the south polar ozone hole is similarly well represented in the two nudged simulations (in particular in EVAL2) which use ECMWF data for the SSTs and do not apply nudging in the stratosphere. Both the ECMWF and ACCMIP SSTs seem to enforce dynamical conditions that allow more realistic ozone destruction in the south polar vortex during southern spring.

## Quantitative evaluation of ozone and selected climate parameters in EMAC

M. Righi et al.

Title Page

Abstract

Introduction

Conclusions

References

Tables

Figures



Back

Close

Full Screen / Esc

Printer-friendly Version

Interactive Discussion







The local maximum between Africa and South America, a region affected by biomass burning emission, is reproduced in all simulations although it is slightly underestimated by the QCTM simulation and overestimated by all other.

The annual cycle is overall well reproduced by the EMAC simulations, showing two distinct maxima during spring in the SH and during spring/summer in the NH. This seasonal increase in tropospheric column ozone is due to an increase of photo-chemical production and stratosphere–troposphere exchange (de Laat et al., 2005; Ziemke et al., 2006). It varies among the EMAC simulations also because of the difference in emissions. Furthermore, single year emissions in the time slice model simulations compared to transient emissions in the nudged and QCTM simulations lead to some differences in emission totals of ozone precursors (see Table S2), with subsequent impacts on tropospheric ozone formation.

### 6.2.3 Vertical ozone profiles

Similar to Fig. 6 in Young et al. (2013), Fig. 15 compares EMAC to ozonesonde data from Tilmes et al. (2012) in three regions (tropics, NH and SH extratropics) and at three altitude levels (250, 500, and 700 hPa). The Tilmes et al. (2012) regional ozonesonde data contain 9 regions: 6 are located in the NH extratropics, 1 in the SH tropics and 2 in the SH extratropics. The tropical region contains mainly data from the SH tropics and only one station, close to the equator in the NH tropics (about 5° N), therefore this region is considered to be the SH tropics.

The comparison shows that the high bias in tropospheric column ozone in the AC-CMIP simulation that was identified in the previous section stems mainly from the 250 and 500 hPa level in the tropics, whereas at 700 hPa and in the NH and SH extratropics the agreement with the ozonesonde data is good. This is similar for the EVAL2 and TS2000 simulation, but the QCTM simulation actually shows a small but negative bias in the tropics at the two levels. As discussed in Sect. 6.2.2, the difference in the simulation can likely be attributed to the difference in lightning NO<sub>x</sub> emissions.

## Quantitative evaluation of ozone and selected climate parameters in EMAC

M. Righi et al.

Title Page

Abstract

Introduction

Conclusions

References

Tables

Figures



Back

Close

Full Screen / Esc

Printer-friendly Version

Interactive Discussion























that are made available to the community. All diagnostics and performance metrics shown in this paper are now implemented in the Earth System Model Validation Tool (ESMValTool). They can be routinely reproduced and applied to new EMAC simulations or other ESMs such as those participating in CCMI (Eyring et al., 2013b) or the Coupled  
5 Model Intercomparison Project (Meehl et al., 2014).

## Appendix A: Statistical measures for quantitative model evaluation

### A1 Root-mean-square difference and overall mean bias

The root-mean-square difference (RMSD), which is commonly used to quantify performance of climate and numerical weather forecast models, is defined as follows:

$$10 \text{ RMSD}_m = \sqrt{\frac{1}{W} \sum_{ijk} w_{ijk} (M_{ijk} - O_{ijk})^2} \quad (\text{A1})$$

where the index  $m$  indicates the model simulation. The fields  $M_{ijk}$  and  $O_{ijk}$  are the model and observation fields, respectively. They can be a function of latitude ( $i$ ), longitude ( $j$ ) and time ( $k$ ), depending on the diagnostic considered. The weights  $w_{ijk}$  are proportional to the grid area when the considered diagnostic is a latitude-longitude map, or to the length of each month when the diagnostic is a monthly time-series (or monthly climatology). The weight are normalized by their sum  $W$ .  
15

This metric has been considered (among others) by Taylor (2001), Jöckel et al. (2006), Gleckler et al. (2008), Reichler and Kim (2008), Karpechko et al. (2010) and Yokoi et al. (2011). While Taylor (2001) and Yokoi et al. (2011) did not consider any weighting, Gleckler et al. (2008), Reichler and Kim (2008) and Karpechko et al. (2010) use the weighting described above. Additionally, Reichler and Kim (2008) weighted the sum also by a factor indirectly proportional to the variance from the observation (thus stressing the variables with lower variance), and Karpechko et al. (2010) by a factor  
20

indirectly proportional to the uncertainty in the observed variable (thus laying stress on more accurate observations). Jöckel et al. (2006) apply a weighting depending on the model error (standard deviation from the averaged value) and the measurement error (combination of instrumental error and variance), thereby giving more importance to values with a smaller total error. Although the latter weightings are reasonable, they are only applicable consistently if all the errors and uncertainties are known.

Additionally the overall mean bias is calculated according to:

$$b_m = \langle M_{ijk} \rangle - \langle O_{ijk} \rangle = \frac{1}{W} \sum_{ijk} w_{ijk} (M_{ijk} - O_{ijk}) \quad (\text{A2})$$

Hence, the overall mean bias  $b_m$  is the difference of the weighted means of the model and of observational fields.

Finally, in order to be able to focus on relative performance among the different EMAC simulations, we normalize the RMSD and the overall mean bias by dividing through the average across the  $m$  individual model simulations (i.e., the model-mean-metrics  $\overline{\text{RMSD}}$  and  $\overline{b}$  defined below) similar to Reichler and Kim (2008) and Karpechko et al. (2010):

$$\overline{\text{RMSD}} = \frac{1}{M} \sum_{m=1}^M \text{RMSD}_m \quad (\text{A3})$$

$$\overline{b} = \frac{1}{M} \sum_{m=1}^M |b_m| \quad (\text{A4})$$

For the interpretation of the portrait diagrams, it should be noted that the RMSD gives positive values only (due to squaring), whereas the overall mean bias is also sensitive to the sign of the deviation, being positive (negative) when the model overestimates (underestimates) the observations. The better the model performance and thus agreement with observations are, the smaller the absolute statistical values. This is different

## Quantitative evaluation of ozone and selected climate parameters in EMAC

M. Righi et al.

Title Page

Abstract

Introduction

Conclusions

References

Tables

Figures

◀

▶

◀

▶

Back

Close

Full Screen / Esc

Printer-friendly Version

Interactive Discussion



to Gleckler et al. (2008), who normalized their metrics by subtracting the model-mean-metric before dividing by the latter  $((b_m - \bar{b})/\bar{b} = b_m/\bar{b} - 1)$  in which case a value of 0 means that the model is equal to the multi-model-mean metric. It also differs from Yokoi et al. (2011), who normalized the metrics by subtracting the model-mean and then dividing by the inter-model standard deviation.

## A2 Taylor diagram

A further possibility to graphically summarize how closely a set of modelled patterns matches observations is provided by the so called Taylor diagram, which was originally proposed by Taylor (2001) and used in many studies (IPCC, 2001; SPARC-CCMVal, 2010) to judge the relative skills of many different models. Since then, it is routinely employed in comparison investigations (e.g., Jöckel et al., 2006; Gleckler et al., 2008). The Taylor diagram is a polar grid plot where the radial coordinate refers to the standard deviation of the model (test) field:

$$\sigma_m = \sqrt{\frac{1}{W} \sum_{ijk} w_{ijk} (M_{ijk} - \langle M_{ijk} \rangle)^2}, \quad (\text{A5})$$

normalized to the standard deviation of the observed (reference) field:

$$\sigma_o = \sqrt{\frac{1}{W} \sum_{ijk} w_{ijk} (O_{ijk} - \langle O_{ijk} \rangle)^2} \quad (\text{A6})$$

The angular coordinate is defined by the inverse cosine of the correlation  $R_m$  between model and observation which is defined as follows:

$$R_m = \frac{\frac{1}{W} \sum_{ijk} w_{ijk} \tilde{M}_{ijk} \tilde{O}_{ijk}}{\sigma_m \sigma_o} \quad (\text{A7})$$

where  $\tilde{M}_{ijk} = M_{ijk} - \langle M_{ijk} \rangle$  and  $\tilde{O}_{ijk} = O_{ijk} - \langle O_{ijk} \rangle$ .

Thus, each model and each diagnostic will provide a distinct point on the diagram. The closer the position of this point to the reference position of the observation ( $\sigma_m/\sigma_o = 1$ ,  $R = 1$  and thus  $\arccos(R) = 0$ ), the better the agreement to the observation. The distance between this point and the reference position is thereby the centred root mean square difference  $c\text{RMSD}_m$ :

$$c\text{RMSD}_m = \sqrt{\frac{1}{W} \sum_{ijk} w_{ijk} (\tilde{M}_{ijk} - \tilde{O}_{ijk})^2}, \quad (\text{A8})$$

Note that the statistics given above are not independent, particularly, adding the centred RMSD and the overall mean bias  $b$  quadratically gives the mean square difference:

$$\text{RMSD}_m^2 = b_m^2 + c\text{RMSD}_m^2 \quad (\text{A9})$$

The correlation  $R_m$  reaches its maximum value of 1 if the two fields have the same pattern of variation ( $\tilde{M}_{ijk} \propto \tilde{O}_{ijk}$  for all  $i, j$  and  $k$ ), however, it does not reveal whether the two fields have the same amplitude of variation (i.e. the proportionality constant between the variation patterns). This amplitude of variation is, however, determined by the standard deviations  $\sigma_m$  and  $\sigma_o$ . Thus, the Taylor diagram contains all the information needed to compare the pattern and amplitude of variation of two fields, and helps indicate which of them (the pattern or the amplitude) has a bigger share in the centred root mean square difference  $c\text{RMSD}$ .

### A3 Welch's $t$ test

Additionally to the already mentioned statistics, the Welch's  $t$  test (an extension of Student's  $t$  test for samples with unequal variances) is applied to the diagnostics where differences between a model and a reference is calculated. This test shows whether two uni-variate variables have an equal mean via a null hypothesis (von Storch and Zwiers, 1984).

**Quantitative  
evaluation of ozone  
and selected climate  
parameters in EMAC**

M. Righi et al.

Title Page

Abstract

Introduction

Conclusions

References

Tables

Figures

◀

▶

◀

▶

Back

Close

Full Screen / Esc

Printer-friendly Version

Interactive Discussion



The difference of the mean between two variables  $X_1$  and  $X_2$  is expressed in dimensionless units as:

$$t = \frac{\bar{X}_1 - \bar{X}_2}{\sqrt{\sigma_1^2/n_1 + \sigma_2^2/n_2}} \quad (\text{A10})$$

- 5 where  $\sigma$  indicates the standard deviation with respect to interannual variability and  $n$  the number of years in each variable.

**The Supplement related to this article is available online at doi:10.5194/gmdd-7-6549-2014-supplement.**

10 *Acknowledgements.* This work was funded by the German Aerospace Center (DLR) Earth System Model Validation (ESMVal) project. The implementation of the performance metrics and diagnostics into the Earth System Model Validation Tool (ESMValTool) was also supported by the European Commission's 7th Framework Programme, under Grant Agreement number 282672, Earth system Model Bias Reduction and assessing Abrupt Climate change (EMBRACE) project. We thank Diego Loyola (DLR, Germany) for providing the GOME data and Chiara Cagnazzo and the entire CMCC climate model group from the Centro Euro-Mediterraneo sui Cambiamenti Climatici (Bologna, Italy), for providing us with SSTs and SICs from their CMIP5 model simulations. Thanks also go to Martin Evaldsson (SMHI, Sweden) for his valuable technical support on the ESMValTool and to Hella Garny (DLR, Germany) for her helpful suggestions on the manuscript draft.

20 The service charges for this open access publication have been covered by a Research Centre of the Helmholtz Association.

## References

- Aumann, H., Chahine, M., Gautier, C., Goldberg, M., Kalnay, E., McMillin, L., Revercomb, H., Rosenkranz, P., Smith, W., Staelin, D., Strow, L., and Susskind, J.: AIRS/AMSU/HSB on the Aqua mission: design, science objectives, data products, and processing systems, *IEEE T. Geosci. Remote*, 41, 253–264, doi:10.1109/TGRS.2002.808356, 2003. 6561
- 5 Bodeker, G. E., Shiona, H., and Eskes, H.: Indicators of Antarctic ozone depletion, *Atmos. Chem. Phys.*, 5, 2603–2615, doi:10.5194/acp-5-2603-2005, 2005. 6562, 6607
- Brühl, C., Drayson, S. R., Russell, J. M., Crutzen, P. J., McInerney, J. M., Purcell, P. N., Claude, H., Gernandt, H., McGee, T. J., McDermid, I. S., and Gunson, M. R.: Halogen occultation experiment ozone channel validation, *J. Geophys. Res.*, 101, 10217–10240, doi:10.1029/95JD02031, 1996. 6561
- 10 Butchart, N., Scaife, A., Bourqui, M., Grandpré, J., Hare, S., Kettleborough, J., Langematz, U., Manzini, E., Sassi, F., Shibata, K., Shindell, D., and Sigmond, M.: Simulations of anthropogenic change in the strength of the Brewer–Dobson circulation, *Clim. Dynam.*, 27, 727–741, doi:10.1007/s00382-006-0162-4, 2006. 6552
- 15 Butchart, N., Cionni, I., Eyring, V., Shepherd, T. G., Waugh, D. W., Akiyoshi, H., Austin, J., Brühl, C., Chipperfield, M. P., Cordero, E., Dameris, M., Deckert, R., Dhomse, S., Frith, S. M., Garcia, R. R., Gettelman, A., Giorgetta, M. A., Kinnison, D. E., Li, F., Mancini, E., McLandress, C., Pawson, S., Pitari, G., Plummer, D. A., Rozanov, E., Sassi, F., Scinocca, J. F., Shibata, K., Steil, B., and Tian, W.: Chemistry-climate model simulations of twenty-first century stratospheric climate and circulation changes, *J. Climate*, 23, 5349–5374, doi:10.1175/2010JCLI3404.1, 2010. 6552
- 20 Butkovskaya, N., Kukui, A., and Le Bras, G.:  $\text{HNO}_3$  forming channel of the  $\text{HO}_2 + \text{NO}$  reaction as a function of pressure and temperature in the ranges of 72–600 Torr and 223–323 K, *J. Phys. Chem. A*, 111, 9047–9053, doi:10.1021/jp074117m, 2007. 6581, 6585
- 25 Butkovskaya, N., Rayez, M.-T., Rayez, J.-C., Kukui, A., and Le Bras, G.: Water vapor effect on the  $\text{HNO}_3$  yield in the  $\text{HO}_2 + \text{NO}$  reaction: experimental and theoretical evidence, *J. Phys. Chem. A*, 113, 11327–11342, doi:10.1021/jp811428p, PMID: 19780600, 2009. 6581
- 30 Cionni, I., Eyring, V., Lamarque, J. F., Randel, W. J., Stevenson, D. S., Wu, F., Bodeker, G. E., Shepherd, T. G., Shindell, D. T., and Waugh, D. W.: Ozone database in support of CMIP5 simulations: results and corresponding radiative forcing, *Atmos. Chem. Phys.*, 11, 11267–11292, doi:10.5194/acp-11-11267-2011, 2011. 6551

**Quantitative  
evaluation of ozone  
and selected climate  
parameters in EMAC**

M. Righi et al.

Title Page

Abstract

Introduction

Conclusions

References

Tables

Figures



Back

Close

Full Screen / Esc

Printer-friendly Version

Interactive Discussion





## Quantitative evaluation of ozone and selected climate parameters in EMAC

M. Righi et al.

Title Page

Abstract

Introduction

Conclusions

References

Tables

Figures



Back

Close

Full Screen / Esc

Printer-friendly Version

Interactive Discussion



dell, D. T., Sudo, K., Szopa, S., and Watanabe, S.: Long-term ozone changes and associated climate impacts in CMIP5 simulations, *J. Geophys. Res.*, 118, 5029–5060, doi:10.1002/jgrd.50316, 2013a. 6552

Eyring, V., Lamarque, J.-F., Hess, P., Arfeuille, F., Bowman, K., Chipperfield, M. P., Duncan, B., Fiore, A., Gettelman, A., Giorgetta, M. A., Granier, C., Hegglin, M., Kinnison, D., Kunze, M., Langematz, U., Luo, B., Martin, R., Matthes, K., Newman, P. A., Peter, T., Robock, A., Ryerson, T., Saiz-Lopez, A., Salawitch, R., Schultz, M., Shepherd, T. G., Shindell, D., Stählerlin, J., Tegtmeier, S., Thomason, L., Tilmes, S., Vernier, J.-P., Waugh, D. W., and Young, P. J.: Overview of IGAC/SPARC Chemistry-Climate Model Initiative (CCMI) community simulations in support of upcoming ozone and climate assessments, *SPARC Newsletter*, 40, 48–66, 2013b. 6586, 6587

Fiore, A. M., Naik, V., Spracklen, D. V., Steiner, A., Unger, N., Prather, M., Bergmann, D., Cameron-Smith, P. J., Cionni, I., Collins, W. J., Dalsøren, S., Eyring, V., Folberth, G. A., Ginoux, P., Horowitz, L. W., Josse, B., Lamarque, J.-F., MacKenzie, I. A., Nagashima, T., O'Connor, F. M., Righi, M., Rumbold, S. T., Shindell, D. T., Skeie, R. B., Sudo, K., Szopa, S., Takemura, T., and Zeng, G.: Global air quality and climate., *Chem. Soc. Rev.*, 41, 6663–6683, doi:10.1039/c2cs35095e, 2012. 6558

Garny, H., Dameris, M., and Stenke, A.: Impact of prescribed SSTs on climatologies and long-term trends in CCM simulations, *Atmos. Chem. Phys.*, 9, 6017–6031, doi:10.5194/acp-9-6017-2009, 2009. 6573

Gettelman, A., Birner, T., Eyring, V., Akiyoshi, H., Bekki, S., Brühl, C., Dameris, M., Kinnison, D. E., Lefevre, F., Lott, F., Mancini, E., Pitari, G., Plummer, D. A., Rozanov, E., Shibata, K., Stenke, A., Struthers, H., and Tian, W.: The Tropical Tropopause Layer 1960–2100, *Atmos. Chem. Phys.*, 9, 1621–1637, doi:10.5194/acp-9-1621-2009, 2009. 6567

Gettelman, A., Eyring, V., Fischer, C., Shiona, H., Cionni, I., Neish, M., Morgenstern, O., Wood, S. W., and Li, Z.: A community diagnostic tool for chemistry climate model validation, *Geosci. Model Dev.*, 5, 1061–1073, doi:10.5194/gmd-5-1061-2012, 2012. 6559

GEWEX-news: February 2011, vol. 21, No. 1, available at: [http://www.gewex.org/gewex\\_nwsltr.html](http://www.gewex.org/gewex_nwsltr.html) (last access: 2 October 2014), 2011. 6562

Giorgetta, M. A. and Bengtsson, L.: Potential role of the quasi-biennial oscillation in the stratosphere–troposphere exchange as found in water vapor in general circulation model experiments, *J. Geophys. Res.*, 104, 6003–6019, doi:10.1029/1998JD200112, 1999. 6556, 6605

## Quantitative evaluation of ozone and selected climate parameters in EMAC

M. Righi et al.

Title Page

Abstract

Introduction

Conclusions

References

Tables

Figures

◀

▶

◀

▶

Back

Close

Full Screen / Esc

Printer-friendly Version

Interactive Discussion



Gleckler, P. J., Taylor, K. E., and Doutriaux, C.: Performance metrics for climate models, *J. Geophys. Res.*, 113, D06104, doi:10.1029/2007JD008972, 2008. 6559, 6561, 6564, 6570, 6587, 6589, 6607

GLOBALVIEW-CO2: Cooperative Atmospheric Data Integration Project – Carbon Dioxide, CD-ROM, NOAA ESRL, Boulder, Colorado, available at: ftp://ftp.cmdl.noaa.gov (last access: 2 October 2014), 2010. 6564, 6607

Gottschaldt, K., Voigt, C., Jöckel, P., Righi, M., Deckert, R., and Dietmüller, S.: Global sensitivity of aviation NO<sub>x</sub> effects to the HNO<sub>3</sub>-forming channel of the HO<sub>2</sub>+NO reaction, *Atmos. Chem. Phys.*, 13, 3003–3025, doi:10.5194/acp-13-3003-2013, 2013. 6578, 6581, 6582

Grewe, V., Brunner, D., Dameris, M., Grenfell, J., Hein, R., Shindell, D., and Staehelin, J.: Origin and variability of upper tropospheric nitrogen oxides and ozone at northern mid-latitudes, *Atmos. Environ.*, 35, 3421–3433, doi:10.1016/S1352-2310(01)00134-0, 2001. 6605

Groß, J.-U. and Russell III, James M.: Technical note: A stratospheric climatology for O<sub>3</sub>, H<sub>2</sub>O, CH<sub>4</sub>, NO<sub>x</sub>, HCl and HF derived from HALOE measurements, *Atmos. Chem. Phys.*, 5, 2797–2807, doi:10.5194/acp-5-2797-2005, 2005. 6561

Harries, J. E., Russell, J. M., Tuck, A. F., Gordley, L. L., Purcell, P., Stone, K., Bevilacqua, R. M., Gunson, M., Nedoluha, G., and Traub, W. A.: Validation of measurements of water vapor from the Halogen Occultation Experiment (HALOE), *J. Geophys. Res.*, 101, 10205–10216, doi:10.1029/95JD02933, 1996. 6561

Hoor, P., Borken-Kleefeld, J., Caro, D., Dessens, O., Endresen, O., Gauss, M., Grewe, V., Hauglustaine, D., Isaksen, I. S. A., Jöckel, P., Lelieveld, J., Myhre, G., Meijer, E., Olivier, D., Prather, M., Schnadt Poberaj, C., Shine, K. P., Staehelin, J., Tang, Q., van Aardenne, J., van Velthoven, P., and Sausen, R.: The impact of traffic emissions on atmospheric ozone and OH: results from QUANTIFY, *Atmos. Chem. Phys.*, 9, 3113–3136, doi:10.5194/acp-9-3113-2009, 2009. 6556, 6557

IPCC: Climate Change 2001: The Scientific Basis, Contribution of Working Group I to the Third Assessment Report of the Intergovernmental Panel on Climate Change, edited by: Houghton, J. T., Ding, Y., Griggs, D. J., Noguer, M., van der Linden, P. J., Dai, X., Maskell, K., and Johnson, C. A., Cambridge University Press, Cambridge, UK, 2001. 6589

IPCC: Climate Change 2007: The Physical Science Basis. Contribution of Working Group I to the Fourth Assessment Report of the Intergovernmental Panel on Climate Change, edited by: Solomon, S., Qin, D., Manning, M., Chen, Z., Marquis, M., Averyt, K. B., Tignor, M., and



## Quantitative evaluation of ozone and selected climate parameters in EMAC

M. Righi et al.

Title Page

Abstract

Introduction

Conclusions

References

Tables

Figures

◀

▶

◀

▶

Back

Close

Full Screen / Esc

Printer-friendly Version

Interactive Discussion



- Kirner, O., Ruhnke, R., Buchholz-Dietsch, J., Jöckel, P., Brühl, C., and Steil, B.: Simulation of polar stratospheric clouds in the chemistry-climate-model EMAC via the submodel PSC, *Geosci. Model Dev.*, 4, 169–182, doi:10.5194/gmd-4-169-2011, 2011. 6605
- Lamarque, J.-F., Bond, T. C., Eyring, V., Granier, C., Heil, A., Klimont, Z., Lee, D., Liousse, C., Mieville, A., Owen, B., Schultz, M. G., Shindell, D., Smith, S. J., Stehfest, E., Van Aardenne, J., Cooper, O. R., Kainuma, M., Mahowald, N., McConnell, J. R., Naik, V., Riahi, K., and van Vuuren, D. P.: Historical (1850–2000) gridded anthropogenic and biomass burning emissions of reactive gases and aerosols: methodology and application, *Atmos. Chem. Phys.*, 10, 7017–7039, doi:10.5194/acp-10-7017-2010, 2010. 6556, 6584, 6586
- Lamarque, J.-F., Shindell, D. T., Josse, B., Young, P. J., Cionni, I., Eyring, V., Bergmann, D., Cameron-Smith, P., Collins, W. J., Doherty, R., Dalsoren, S., Faluvegi, G., Folberth, G., Ghan, S. J., Horowitz, L. W., Lee, Y. H., MacKenzie, I. A., Nagashima, T., Naik, V., Plummer, D., Righi, M., Rumbold, S. T., Schulz, M., Skeie, R. B., Stevenson, D. S., Strode, S., Sudo, K., Szopa, S., Voulgarakis, A., and Zeng, G.: The Atmospheric Chemistry and Climate Model Intercomparison Project (ACCMIP): overview and description of models, simulations and climate diagnostics, *Geosci. Model Dev.*, 6, 179–206, doi:10.5194/gmd-6-179-2013, 2013. 6558
- Landgraf, J. and Crutzen, P. J.: An efficient method for online calculations of photolysis and heating rates, *J. Atmos. Sci.*, 55, 863–878, doi:10.1175/1520-0469(1998)055<0863:AEMFOC>2.0.CO;2, 1998. 6605
- Lin, S.-J., and Rood, R. B.: Multidimensional flux-form semi-Lagrangian transport schemes, *Mon. Weather Rev.*, 124, 2046–2070, doi:10.1175/1520-0493(1996)124<2046:MFFSLT>2.0.CO;2, 1996. 6554
- Logan, J. A.: An analysis of ozonesonde data for the troposphere: recommendations for testing 3-D models and development of a gridded climatology for tropospheric ozone, *J. Geophys. Res.*, 104, 16115–16149, doi:10.1029/1998JD100096, 1999. 6563
- Loyola, D. and Coldewey-Egbers, M.: Multi-sensor data merging with stacked neural networks for the creation of satellite long-term climate data records, *EURASIP J. Adv. Sig. Pr.*, 2012, 1–10, doi:10.1186/1687-6180-2012-91, 2012. 6562, 6607
- Loyola, D. G., Coldewey-Egbers, R. M., Dameris, M., Garny, H., Stenke, A., Van Roozendaal, M., Lerot, C., Balis, D., and Koukouli, M.: Global long-term monitoring of the ozone layer – a prerequisite for predictions, *Int. J. Remote Sens.*, 30, 4295–4318, doi:10.1080/01431160902825016, 2009. 6562, 6607

## Quantitative evaluation of ozone and selected climate parameters in EMAC

M. Righi et al.

Title Page

Abstract

Introduction

Conclusions

References

Tables

Figures

◀

▶

◀

▶

Back

Close

Full Screen / Esc

Printer-friendly Version

Interactive Discussion



- Masarie, K. A. and Tans, P. P.: Extension and integration of atmospheric carbon dioxide data into a globally consistent measurement record, *J. Geophys. Res.*, 100, 11593–11610, doi:10.1029/95JD00859, 1995. 6564
- 5 Meehl, G. A., Moss, R., Taylor, K. E., Eyring, V., Stouffer, R. J., Bony, S., and Stevens, B.: Climate model intercomparisons: preparing for the next phase, *Trans. Am. Geophys. Union*, 95, 77–78, doi:10.1002/2014EO090001, 2014. 6587
- 10 Moss, R. H., Edmonds, J. A., Hibbard, K. A., Manning, M. R., Rose, S. K., van Vuuren, D. P., Carter, T. R., Emori, S., Kainuma, M., Kram, T., Meehl, G. A., Mitchell, J. F. B., Nakicenovic, N., Riahi, K., Smith, S. J., Stouffer, R. J., Thomson, A. M., Weyant, J. P., and Wilbanks, T. J.: The next generation of scenarios for climate change research and assessment., *Nature*, 463, 747–756, doi:10.1038/nature08823, 2010. 6551
- 15 Naik, V., Voulgarakis, A., Fiore, A. M., Horowitz, L. W., Lamarque, J.-F., Lin, M., Prather, M. J., Young, P. J., Bergmann, D., Cameron-Smith, P. J., Cionni, I., Collins, W. J., Dalsøren, S. B., Doherty, R., Eyring, V., Faluvegi, G., Folberth, G. A., Josse, B., Lee, Y. H., MacKenzie, I. A., Nagashima, T., van Noije, T. P. C., Plummer, D. A., Righi, M., Rumbold, S. T., Skeie, R., Shindell, D. T., Stevenson, D. S., Strode, S., Sudo, K., Szopa, S., and Zeng, G.: Preindustrial to present-day changes in tropospheric hydroxyl radical and methane lifetime from the Atmospheric Chemistry and Climate Model Intercomparison Project (ACCMIP), *Atmos. Chem. Phys.*, 13, 5277–5298, doi:10.5194/acp-13-5277-2013, 2013. 6558, 6578, 6582
- 20 Nordeng, T.-E.: Extended Versions of the Convective Parametrization Scheme at ECMWF and Their Impact on the Mean and Transient Activity of the Model in the Tropics, European Centre for Medium-Range Weather Forecasts, Reading, UK, 1994. 6554
- 25 Park, J. H., Russell, J. M., Gordley, L. L., Drayson, S. R., Benner, D. C., McInerney, J. M., Gunson, M. R., Toon, G. C., Sen, B., Blavier, J.-F., Webster, C. R., Zipf, E. C., Erdman, P., Schmidt, U., and Schiller, C.: Validation of halogen occultation experiment CH<sub>4</sub> measurements from the UARS, *J. Geophys. Res.*, 101, 10183–10203, doi:10.1029/95JD02736, 1996. 6561
- Perlwitz, J., Pawson, S., Fogt, R. L., Nielsen, J. E., and Neff, W. D.: Impact of stratospheric ozone hole recovery on Antarctic climate, *Geophys. Res. Lett.*, 35, L08714, doi:10.1029/2008GL033317, 2008. 6552
- 30 Pozzer, A., Jöckel, P., Sander, R., Williams, J., Ganzeveld, L., and Lelieveld, J.: Technical Note: The MESSy-submodel AIRSEA calculating the air-sea exchange of chemical species, *Atmos. Chem. Phys.*, 6, 5435–5444, doi:10.5194/acp-6-5435-2006, 2006. 6605

**Quantitative  
evaluation of ozone  
and selected climate  
parameters in EMAC**

M. Righi et al.

Title Page

Abstract

Introduction

Conclusions

References

Tables

Figures



Back

Close

Full Screen / Esc

Printer-friendly Version

Interactive Discussion

- Pozzer, A., Jöckel, P., Tost, H., Sander, R., Ganzeveld, L., Kerkweg, A., and Lelieveld, J.: Simulating organic species with the global atmospheric chemistry general circulation model ECHAM5/MESSy1: a comparison of model results with observations, *Atmos. Chem. Phys.*, 7, 2527–2550, doi:10.5194/acp-7-2527-2007, 2007. 6552, 6555, 6577, 6579
- 5 Price, C. and Rind, D.: Modeling global lightning distributions in a general circulation model, *Mon. Weather Rev.*, 122, 1930–1939, doi:10.1175/1520-0493(1994)122<1930:MGLDIA>2.0.CO;2, 1994. 6575, 6605
- Prinn, R. G., Weiss, R. F., Fraser, P. J., Simmonds, P. G., Cunnold, D. M., Aleya, F. N., Doherty, S. O., Salameh, P., Miller, B. R., Huang, J., Wang, R. H. J., Hartley, D. E., Harth, C.,  
10 Steele, L. P., Sturrock, G., Midgley, P. M., and McCulloch, A.: A history of chemically and radiatively important gases in air deduced from ALE/GAGE/AGAGE, *J. Geophys. Res.*, 105, 17751–17792, doi:10.1029/2000JD900141, 2000. 6574
- Räsänen, P., and Järvinen, H.: Impact of cloud and radiation scheme modifications on climate simulated by the ECHAM5 atmospheric GCM, *Q. J. Roy. Meteor. Soc.*, 136, 1733–1752, doi:10.1002/qj.674, 2010. 6572
- 15 Rayner, N. A., Parker, D. E., Horton, E. B., Folland, C. K., Alexander, L. V., Rowell, D. P., Kent, E. C., and Kaplan, A.: Global analyses of sea surface temperature, sea ice, and night marine air temperature since the late nineteenth century, *J. Geophys. Res.*, 108, 4407, doi:10.1029/2002JD002670, 2003. 6557
- 20 Reichler, T. and Kim, J.: How well do coupled models simulate today's climate?, *B. Am. Meteorol. Soc.*, 89, 303–311, doi:10.1175/BAMS-89-3-303, 2008. 6587, 6588
- Roeckner, E., Brokopf, E., Esch, M., Giorgetta, M. A., Hagemann, S., and Kornblueh, L.: Sensitivity of simulated climate to horizontal and vertical resolution in the ECHAM5 atmosphere model, *J. Climate*, 19, 3771–3791, doi:10.1175/JCLI3824.1, 2006. 6553, 6554, 6605
- 25 Russell, J. M., Gordley, L. L., Park, J. H., Drayson, S. R., Hesketh, W. D., Cicerone, R. J., Tuck, A. F., Frederick, J. E., Harries, J. E., and Crutzen, P. J.: The halogen occultation experiment, *J. Geophys. Res.*, 98, 10777–10797, doi:10.1029/93JD00799, 1993. 6561
- Russell, J. M., Deaver, L. E., Luo, M., Park, J. H., Gordley, L. L., Tuck, A. F., Toon, G. C., Gunson, M. R., Traub, W. A., Johnson, D. G., Jucks, K. W., Murcray, D. G., Zander, R.,  
30 Nolt, I. G., and Webster, C. R.: Validation of hydrogen chloride measurements made by the halogen occultation experiment from the UARS platform, *J. Geophys. Res.*, 101, 10151–10162, doi:10.1029/95JD01696, 1996. 6561

## Quantitative evaluation of ozone and selected climate parameters in EMAC

M. Righi et al.

Title Page

Abstract

Introduction

Conclusions

References

Tables

Figures



Back

Close

Full Screen / Esc

Printer-friendly Version

Interactive Discussion



Sander, R., Kerkweg, A., Jöckel, P., and Lelieveld, J.: Technical note: The new comprehensive atmospheric chemistry module MECCA, *Atmos. Chem. Phys.*, 5, 445–450, doi:10.5194/acp-5-445-2005, 2005. 6554, 6605

Sander, R., Baumgaertner, A., Gromov, S., Harder, H., Jöckel, P., Kerkweg, A., Kubistin, D., Regelin, E., Riede, H., Sandu, A., Taraborrelli, D., Tost, H., and Xie, Z.-Q.: The atmospheric chemistry box model CAABA/MECCA-3.0, *Geosci. Model Dev.*, 4, 373–380, doi:10.5194/gmd-4-373-2011, 2011. 6581

Schmitt, A. and Brunner, B.: Emissions from aviation and their development over time, in: *Pollutants from Air Traffic – Results of Atmospheric Research 1992–1997*, edited by: Schumann, U., Chlond, A., Ebel, A., Kärcher, B., Pak, H., Schlager, H., Schmitt, A., and Wendling, P., DLR-Mitteilung 97-04, Deutsches Zentrum für Luft- und Raumfahrt, Cologne, Germany, 37–52, 1997. 6556

Schumann, U. and Huntrieser, H.: The global lightning-induced nitrogen oxides source, *Atmos. Chem. Phys.*, 7, 3823–3907, doi:10.5194/acp-7-3823-2007, 2007. 6575

Shepherd, T. G.: Dynamics, stratospheric ozone, and climate change, *Atmos. Ocean*, 46, 117–138, doi:10.3137/ao.460106, 2008. 6552

Silva, R. A., West, J. J., Zhang, Y., Anenberg, S. C., Lamarque, J.-F., Shindell, D. T., Collins, W. J., Dalsøren, S., Faluvegi, G., Folberth, G., Horowitz, L. W., Nagashima, T., Naik, V., Rumbold, S., Skeie, R., Sudo, K., Takemura, T., Bergmann, D., Cameron-Smith, P., Cionni, I., Doherty, R. M., Eyring, V., Josse, B., MacKenzie, I. A., Plummer, D., Righi, M., Stevenson, D. S., Strode, S., Szopa, S., and Zeng, G.: Global premature mortality due to anthropogenic outdoor air pollution and the contribution of past climate change, *Environ. Res. Lett.*, 8, 034005, doi:10.1088/1748-9326/8/3/034005, 2013. 6558

Son, S.-W., Polvani, L. M., Waugh, D. W., Akiyoshi, H., Garcia, R., Kinnison, D., Pawson, S., Rozanov, E., Shepherd, T. G., and Shibata, K.: The impact of stratospheric ozone recovery on the Southern Hemisphere westerly jet, *Science*, 320, 1486–1489, doi:10.1126/science.1155939, 2008. 6552

Son, S.-W., Gerber, E. P., Perlwitz, J., Polvani, L. M., Gillett, N. P., Seo, K.-H., Eyring, V., Shepherd, T. G., Waugh, D., Akiyoshi, H., Austin, J., Baumgaertner, A., Bekki, S., Braesicke, P., Brühl, C., Butchart, N., Chipperfield, M. P., Cugnet, D., Dameris, M., Dhomse, S., Frith, S., Garny, H., Garcia, R., Hardiman, S. C., Jöckel, P., Lamarque, J. F., Mancini, E., Marchand, M., Michou, M., Nakamura, T., Morgenstern, O., Pitari, G., Plummer, D. A., Pyle, J., Rozanov, E., Scinocca, J. F., Shibata, K., Smale, D., Teyssèdre, H., Tian, W., and Yamashita, Y.: Impact

## Quantitative evaluation of ozone and selected climate parameters in EMAC

M. Righi et al.

Title Page

Abstract

Introduction

Conclusions

References

Tables

Figures



Back

Close

Full Screen / Esc

Printer-friendly Version

Interactive Discussion



- of stratospheric ozone on Southern Hemisphere circulation change: a multimodel assessment, *J. Geophys. Res.*, 115, D00M07, doi:10.1029/2010JD014271, 2010. 6552
- SPARC-CCMVal: SPARC Report on the Evaluation of Chemistry-Climate Models, edited by: Eyring, V., Shepherd, T. G., and Waugh, D. W., SPARC Report No. 5, WCRP-132, WMO/TD-No. 1526, 2010. 6552, 6566, 6584, 6589
- 5 Stenke, A., Grewe, V., and Ponater, M.: Lagrangian transport of water vapor and cloud water in the ECHAM4 GCM and its impact on the cold bias, *Clim. Dynam.*, 31, 491–506, doi:10.1007/s00382-007-0347-5, 2008. 6566
- Stevenson, D. S., Young, P. J., Naik, V., Lamarque, J.-F., Shindell, D. T., Voulgarakis, A., Skeie, R. B., Dalsoren, S. B., Myhre, G., Berntsen, T. K., Folberth, G. A., Rumbold, S. T., Collins, W. J., MacKenzie, I. A., Doherty, R. M., Zeng, G., van Noije, T. P. C., Strunk, A., Bergmann, D., Cameron-Smith, P., Plummer, D. A., Strode, S. A., Horowitz, L., Lee, Y. H., Szopa, S., Sudo, K., Nagashima, T., Josse, B., Cionni, I., Righi, M., Eyring, V., Conley, A., Bowman, K. W., Wild, O., and Archibald, A.: Tropospheric ozone changes, radiative forcing and attribution to emissions in the Atmospheric Chemistry and Climate Model Intercomparison Project (ACCMIP), *Atmos. Chem. Phys.*, 13, 3063–3085, doi:10.5194/acp-13-3063-2013, 2013. 6551, 6558, 6575
- 15 Tanre, D., Geleyn, J.-F., and Slingo, J.: First results of the introduction of an advanced aerosol-radiation interaction in the ECMWF low resolution global model, in: *Aerosols and Their Climatic Effects*, edited by: Gerber, H. and Deepak, A., A. Deepak Publ., 133–177, 1994. 6554
- Taraborrelli, D., Lawrence, M. G., Crowley, J. N., Dillon, T. J., Gromov, S., Grosz, C. B. M., Vereecken, L., and Lelieveld, J.: Hydroxyl radical buffered by isoprene oxidation over tropical forests, *Nat. Geosci.*, 5, 190–193, doi:10.1038/ngeo1405, 2012. 6582
- Taylor, K. E.: Summarizing multiple aspects of model performance in a single diagram, *J. Geophys. Res.*, 106, 7183–7192, doi:10.1029/2000JD900719, 2001. 6587, 6589
- 25 Thompson, D. W. J. and Solomon, S.: Interpretation of recent Southern Hemisphere climate change, *Science*, 296, 895–899, doi:10.1126/science.1069270, 2002. 6552
- Thompson, D. W. J. and Solomon, S.: Recent stratospheric climate trends as evidenced in radiosonde data: global structure and tropospheric linkages, *J. Climate*, 18, 4785–4795, doi:10.1175/JCLI3585.1, 2005. 6552
- 30 Thompson, D. W. J., Baldwin, M. P., and Solomon, S.: Stratosphere–troposphere coupling in the Southern Hemisphere, *J. Climate*, 62, 708–715, doi:10.1175/JAS-3321.1, 2005. 6552

## Quantitative evaluation of ozone and selected climate parameters in EMAC

M. Righi et al.

Title Page

Abstract

Introduction

Conclusions

References

Tables

Figures



Back

Close

Full Screen / Esc

Printer-friendly Version

Interactive Discussion



- Tiedtke, M.: A comprehensive mass flux scheme for cumulus parameterization in large-scale models, *Mon. Weather Rev.*, 117, 1779–1800, doi:10.1175/1520-0493(1989)117<1779:ACMFSF>2.0.CO;2, 1989. 6554
- Tilmes, S., Lamarque, J.-F., Emmons, L. K., Conley, A., Schultz, M. G., Saunois, M., Thouret, V., Thompson, A. M., Oltmans, S. J., Johnson, B., and Tarasick, D.: Technical Note: Ozone sonde climatology between 1995 and 2011: description, evaluation and applications, *Atmos. Chem. Phys.*, 12, 7475–7497, doi:10.5194/acp-12-7475-2012, 2012. 6563, 6576, 6586, 6607, 6623
- Tost, H.: Global modelling of cloud, convection and precipitation influences on trace gases and aerosols, Ph.D. thesis, University of Bonn, Germany, available at: <http://hss.ulb.uni-bonn.de/2006/0731/0731.htm> (last access: 2 October 2014), 2006. 6605
- Tost, H., Jöckel, P., Kerkweg, A., Sander, R., and Lelieveld, J.: Technical note: A new comprehensive SCAVenging submodel for global atmospheric chemistry modelling, *Atmos. Chem. Phys.*, 6, 565–574, doi:10.5194/acp-6-565-2006, 2006a. 6554
- Tost, H., Jöckel, P., and Lelieveld, J.: Influence of different convection parameterisations in a GCM, *Atmos. Chem. Phys.*, 6, 5475–5493, doi:10.5194/acp-6-5475-2006, 2006b. 6605
- van Aalst, M. K., van den Broek, M. M. P., Bregman, A., Brühl, C., Steil, B., Toon, G. C., Garcelon, S., Hansford, G. M., Jones, R. L., Gardiner, T. D., Roelofs, G. J., Lelieveld, J., and Crutzen, P. J.: Trace gas transport in the 1999/2000 Arctic winter: comparison of nudged GCM runs with observations, *Atmos. Chem. Phys.*, 4, 81–93, doi:10.5194/acp-4-81-2004, 2004. 6555
- van Aardenne, J., Dentener, F., Olivier, J., Peters, J., and Ganzeveld, L.: The EDGAR3.2 Fast Track 2000 dataset (32FT2000), Tech. rep., Joint Research Centre, Institute for Environment and Sustainability (JRC-IES), Climate Change Unit, Ispra (VA), Italy, 2005. 6556
- van der Werf, G. R., Randerson, J. T., Giglio, L., Gobron, N., and Dolman, A. J.: Climate controls on the variability of fires in the tropics and subtropics, *Global Biogeochem. Cy.*, 22, GB3028, doi:10.1029/2007GB003122, 2008. 6577
- van der Werf, G. R., Randerson, J. T., Giglio, L., Collatz, G. J., Mu, M., Kasibhatla, P. S., Morton, D. C., DeFries, R. S., Jin, Y., and van Leeuwen, T. T.: Global fire emissions and the contribution of deforestation, savanna, forest, agricultural, and peat fires (1997–2009), *Atmos. Chem. Phys.*, 10, 11707–11735, doi:10.5194/acp-10-11707-2010, 2010. 6556
- von Kuhlmann, R., Lawrence, M. G., Crutzen, P. J., and Rasch, P. J.: A model for studies of tropospheric ozone and nonmethane hydrocarbons: model description and ozone results, *J. Geophys. Res.*, 108, 4294, doi:10.1029/2002JD002893, 2003. 6578, 6580



## GMDD

7, 6549–6627, 2014

### Quantitative evaluation of ozone and selected climate parameters in EMAC

M. Righi et al.

Title Page

Abstract

Introduction

Conclusions

References

Tables

Figures



Back

Close

Full Screen / Esc

Printer-friendly Version

Interactive Discussion





## Quantitative evaluation of ozone and selected climate parameters in EMAC

M. Righi et al.

Title Page

Abstract

Introduction

Conclusions

References

Tables

Figures



Back

Close

Full Screen / Esc

Printer-friendly Version

Interactive Discussion



**Table 2.** Overview of the four EMAC simulations evaluated in this study. All experiments have a spin-up year at the beginning of the simulated period which is not considered in the analysis.

Name	Resolution	Analysed time period	Running mode	SST/SIC
EVAL2	T42L90MA	1999–2009	Nudged, coupled	ECMWF
QCTM	T42L90MA	1999–2007	Nudged, QCTM	ECMWF
TS2000	T42L90MA	10 years under 2000 conditions	Free-running timeslice, coupled	HadISST1
ACCMIP	T42L90MA	10 years under 2000 conditions	Free-running timeslice, coupled	CMCC

## Quantitative evaluation of ozone and selected climate parameters in EMAC

M. Righi et al.

**Table 3.** List of the diagnostics applied in this work and for which a quantitative evaluation based on performance metrics has been applied. The climatological mean field considers both the time (annual cycle) and the space (latitude-longitude) coordinate, or only time in some cases. Regions are defined as follows: Glob (90° N–90° S), Trop (20° N–20° S), NHext (20–90° N), SHext (20–90° S), NHmidlat (35–60° N), SHmidlat (35–60° S), NHpolar (60–90° N), SHpolar (60–90° S). The short name of the diagnostics follows the CMOR standard. The references in the last column are labeled as follows: Bo2005 (Bodeker et al., 2005), GC2010 (GLOBALVIEW-CO<sub>2</sub>, 2010), GI2008 (Gleckler et al., 2008), Lo2009 (Loyola et al., 2009), Lo2012 (Loyola and Coldewey-Egbers, 2012), Ti2000 (Tilmes et al., 2012), Zi2006 (Ziemke et al., 2006), Zi2011 (Ziemke et al., 2011).

Name	Clim. mean field	Level	Region	Observations	Short name	Reference
Temperature	space–time	850 hPa 200 hPa 30 hPa 5 hPa	Glob Trop NHext SHext	Era-Interim (1995–2005) NCEP (1995–2005)	ta_<reg>-<lev>	GI2008
Eastward wind	space–time	850 hPa 200 hPa 30 hPa 5 hPa	Glob Trop NHext SHext	Era-Interim (1995–2005) NCEP (1995–2005)	ua_<reg>-<lev>	GI2008
Northward wind	space–time	850 hPa 200 hPa 30 hPa 5 hPa	Glob Trop NHext SHext	Era-Interim (1995–2005) NCEP (1995–2005)	va_<reg>-<lev>	GI2008
Geopotential height	space–time	850 hPa 500 hPa 30 hPa 5 hPa	Glob Trop NHext SHext	Era-Interim (1995–2005) NCEP (1995–2005)	zg_<reg>-<lev>	GI2008
Specific humidity	space–time	850 hPa 400 hPa 30 hPa 5 hPa	Glob Trop NHext SHext	AIRS (2003–2010) ERA-Interim (1995–2005)	hus_<reg>-<lev>	GI2008

Title Page

Abstract

Introduction

Conclusions

References

Tables

Figures

◀

▶

◀

▶

Back

Close

Full Screen / Esc

Printer-friendly Version

Interactive Discussion



## Quantitative evaluation of ozone and selected climate parameters in EMAC

M. Righi et al.

Title Page

Abstract

Introduction

Conclusions

References

Tables

Figures

◀

▶

◀

▶

Back

Close

Full Screen / Esc

Printer-friendly Version

Interactive Discussion



**Table 3.** Continued.

Name	Clim. mean field	Level	Region	Observations	Short name	Reference
Reflected SW radiation (all-sky)	space–time	–	Glob	SRB (1995–2005) CERES (2001–2005)	rsut_Glob	GI2008
Outgoing LW radiation (all-sky)	space–time	–	Glob	SRB (1995–2005) CERES (2001–2005)	rlut_Glob	GI2008
Outgoing LW radiation (clear-sky)	space–time	–	Glob	SRB (1995–2005) CERES (2001–2005)	rlutcs_Glob	GI2008
Tropospheric ozone	time	700 hPa 500 hPa 250 hPa	Trop NHext SHext	Ozonesondes (1995–2009)	vmro3_<reg>-<lev>	Ti2000
Tropospheric column ozone	space–time	–	Glob Trop NHext SHext	MLS/OMI (2005–2012)	tropoz_<reg>	Zi2006 Zi2011
Total column ozone	space–time	–	Glob Trop NHmidlat SHmidlat NHpolar SHpolar	NIWA (1998–2010) GOME (1998–2010)	toz_<reg>	Bo2005 Lo2009 Lo2012
Surface CO	time	surface	various	GLOBALVIEW (1998–2008)	co_<reg>	GC2010

## Quantitative evaluation of ozone and selected climate parameters in EMAC

M. Righi et al.

Title Page

Abstract

Introduction

Conclusions

References

Tables

Figures



Back

Close

Full Screen / Esc

Printer-friendly Version

Interactive Discussion

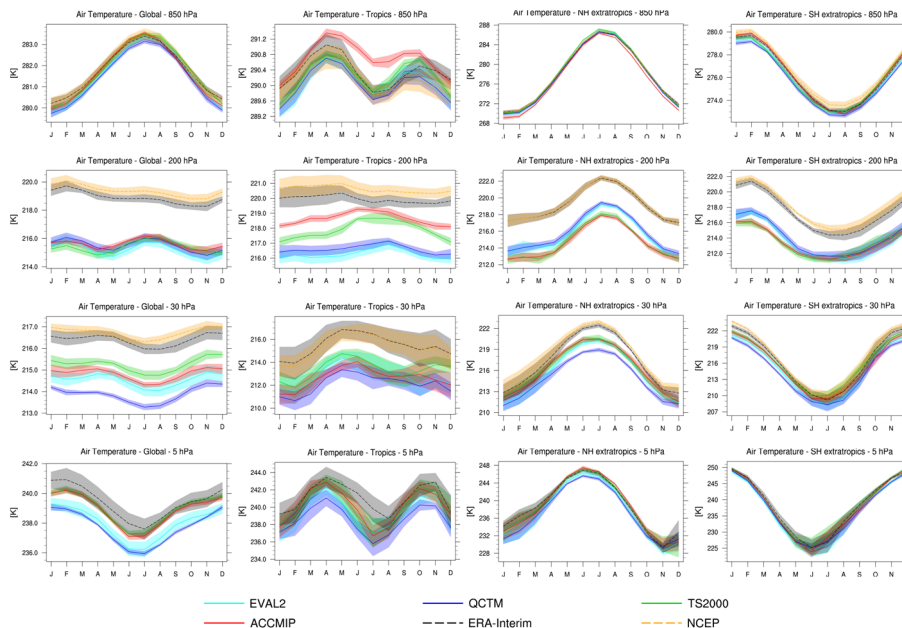


**Figure 1.** Annual cycle of temperature climatology at 850, 200, 30 and 5 hPa averaged globally, over the tropics ( $20^{\circ}$  S– $20^{\circ}$  N), NH extratropics ( $20$ – $90^{\circ}$  N) and SH extratropics ( $20$ – $90^{\circ}$  S) for the EMAC simulations, in comparison to ERA-Interim and NCEP/NCAR reanalysis data. Shaded areas indicate the  $\pm 1\sigma$  interannual variability.

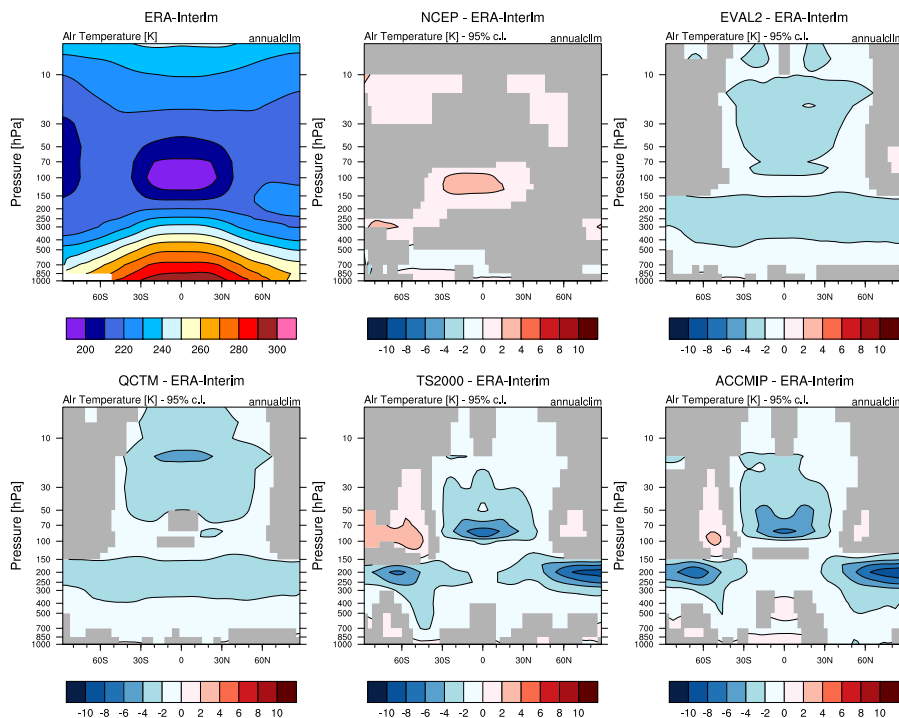


**Figure 2.** Annual mean of zonally averaged temperature profile for the EMAC simulations in comparison to ERA-Interim and NCEP/NCAR reanalysis data. The upper left plot shows ERA-Interim absolute values; all other plots show differences between the model simulations (or NCEP/NCAR) and ERA-Interim. Differences between the two fields which are not statistically significant according to the  $t$  test (95 % confidence level) are masked out in gray.



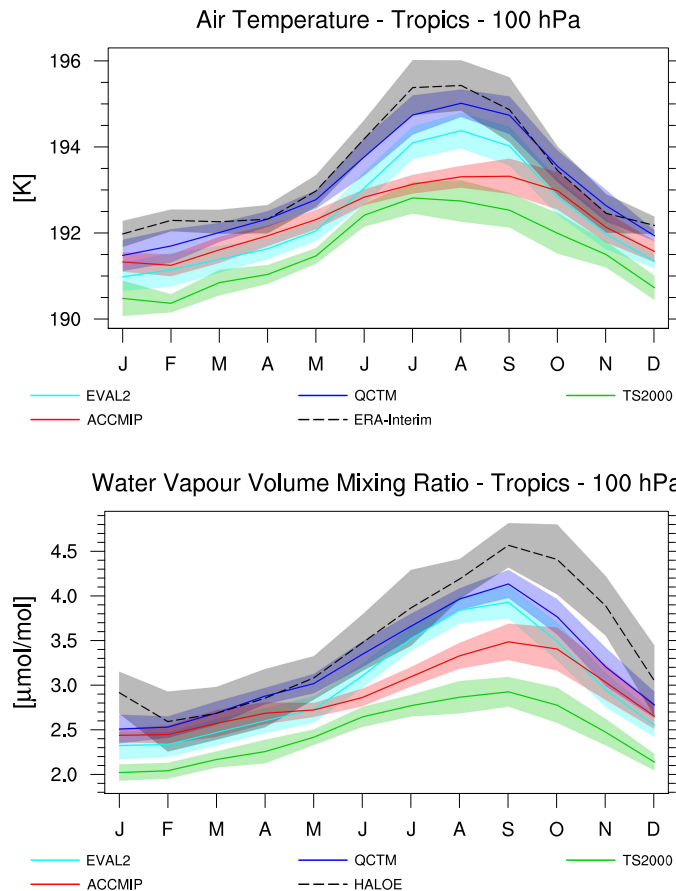


**Figure 4.** Annual cycle of temperature (top) and water vapour (bottom) climatology at 100 hPa averaged over the tropics ( $20^{\circ}\text{N}$ – $20^{\circ}\text{S}$ ) for the EMAC simulations, in comparison to ERA-Interim reanalysis and HALOE data, respectively. Shaded areas indicate the  $\pm 1\sigma$  interannual variability.

## Quantitative evaluation of ozone and selected climate parameters in EMAC

M. Righi et al.

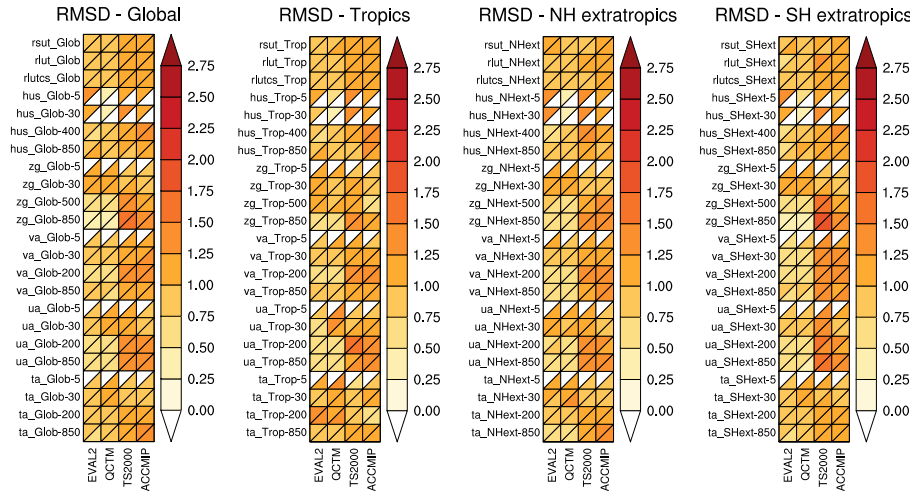


**Figure 5.** Root-mean square difference of the chosen basic climate parameters over the global domain, the tropics, and the NH and SH extratropics (from left to right, respectively). Columns and rows of each panel represent the EMAC simulations and the given diagnostics (see Table 3), respectively. Where an alternative dataset is available, the diagram boxes are split in two parts, showing the model performance compared to the primary (lower triangle) and alternative (upper triangle) dataset. Where no observations are available, the triangles are marked white.

Title Page

[Abstract](#)    [Introduction](#)  
[Conclusions](#)    [References](#)  
[Tables](#)    [Figures](#)

⏪    ⏩  
◀    ▶  
[Back](#)    [Close](#)

[Full Screen / Esc](#)

[Printer-friendly Version](#)

[Interactive Discussion](#)



## Quantitative evaluation of ozone and selected climate parameters in EMAC

M. Righi et al.

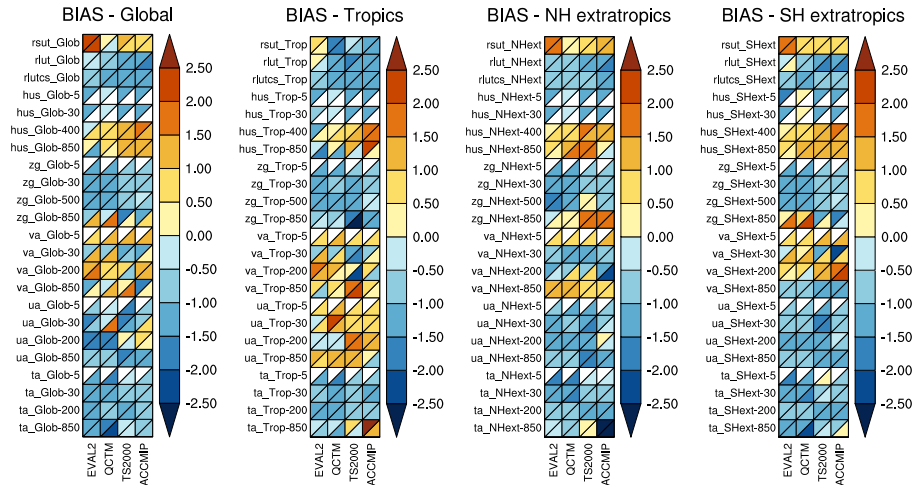


Figure 6. As in Fig. 5, for the overall mean bias.

Title Page

Abstract Introduction

Conclusions References

Tables Figures

◀ ▶

◀ ▶

Back Close

Full Screen / Esc

Printer-friendly Version

Interactive Discussion

## Quantitative evaluation of ozone and selected climate parameters in EMAC

M. Righi et al.

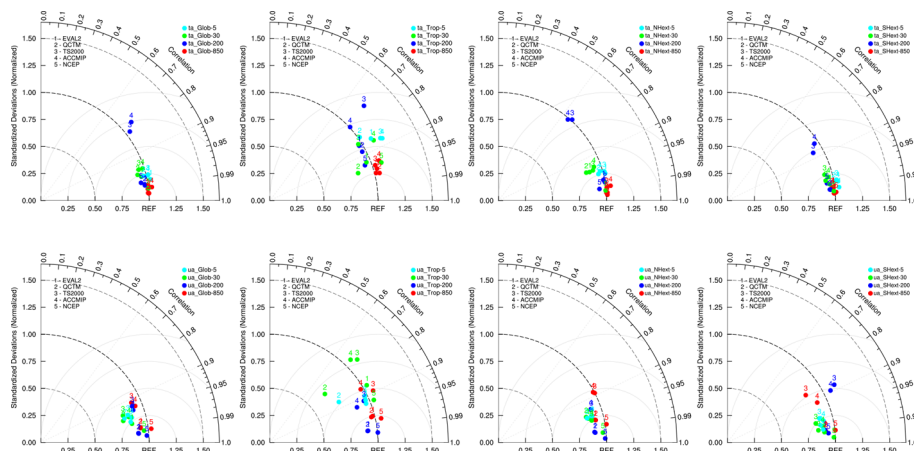


**Figure 7.** Taylor diagrams of temperature (top row) and eastward wind (bottom row) over the four chosen domains (global, tropics, NH and SH extratropics, from left to right, respectively) and height-levels (850, 200, 30, and 5 hPa).

Title Page

Abstract

Introduction

Conclusions

References

Tables

Figures



Back

Close

Full Screen / Esc

Printer-friendly Version

Interactive Discussion

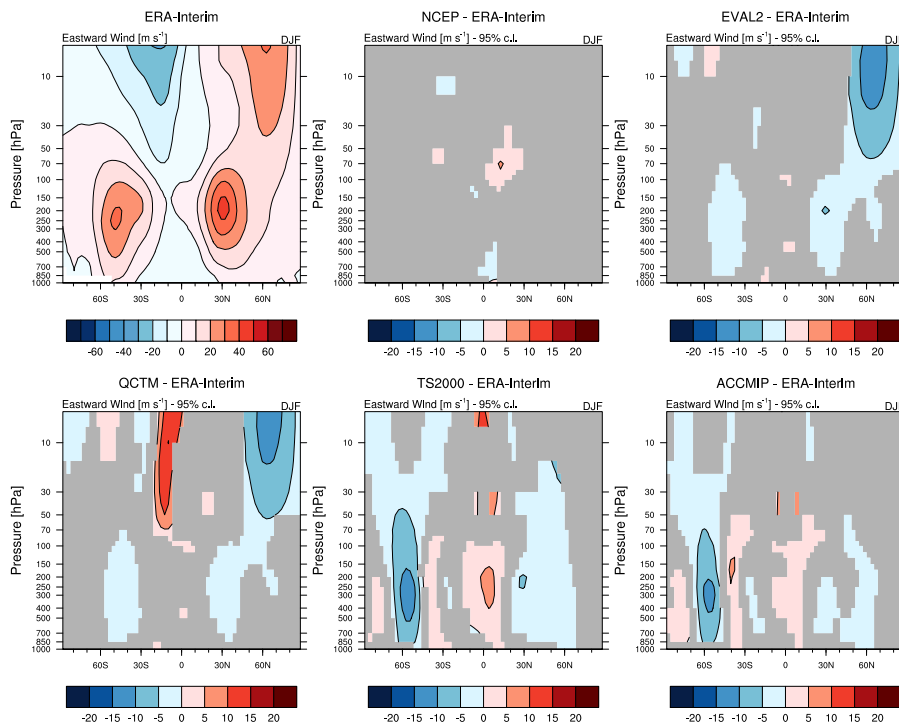


**Figure 8.** Seasonal (DJF) mean of zonally averaged eastward wind profile for the EMAC simulations in comparison to ERA-Interim and NCEP/NCAR reanalysis data. The upper left plot shows ERA-Interim absolute values; all other plots show differences between the model simulations (or NCEP/NCAR) and ERA-Interim. Differences between the two fields which are not statistically significant according to the  $t$  test (95 % confidence level) are masked out in gray.

## Quantitative evaluation of ozone and selected climate parameters in EMAC

M. Righi et al.

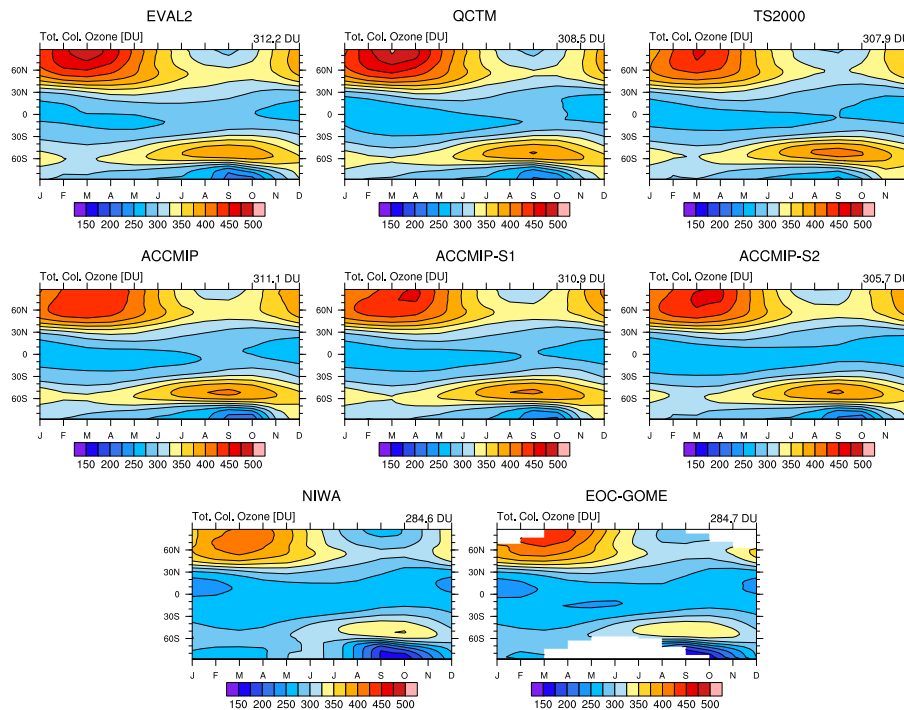


**Figure 9.** Total column ozone climatology for the EMAC simulations compared to the NIWA combined total column ozone database and GOME data. The values on top of each panel show the global (area-weighted) average, calculated after regridding the data to the horizontal grid of the model and ignoring the grid cells without available observational data in the GOME dataset.

Title Page

Abstract

Introduction

Conclusions

References

Tables

Figures

⏪

⏩

◀

▶

Back

Close

Full Screen / Esc

Printer-friendly Version

Interactive Discussion





## Quantitative evaluation of ozone and selected climate parameters in EMAC

M. Righi et al.

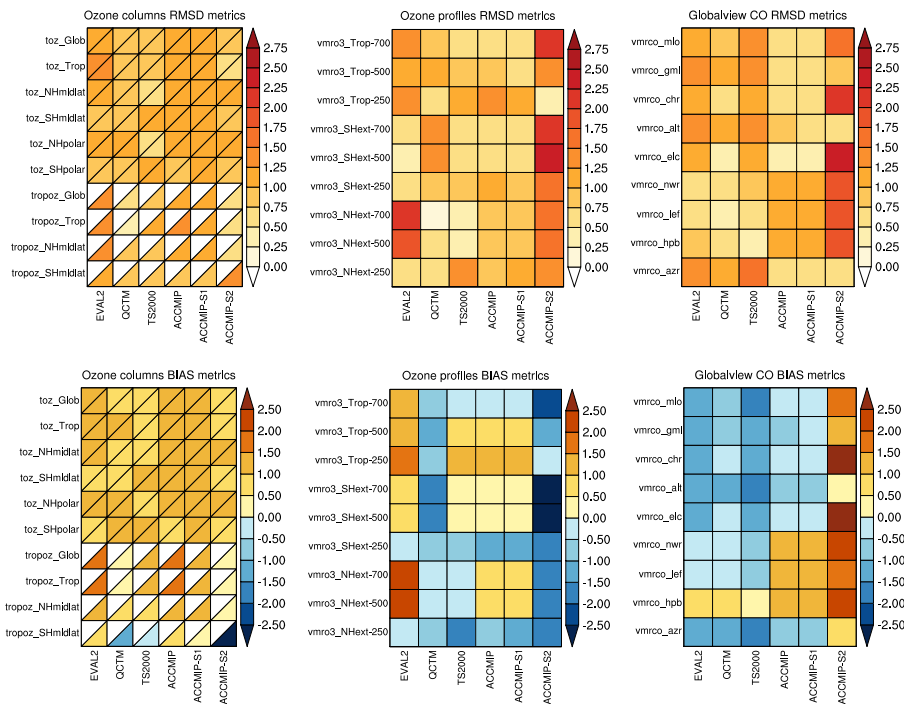


**Figure 11.** Root-mean square difference (top) and overall mean bias (bottom) for total and tropospheric column ozone (left), ozonesondes (middle) and surface CO diagnostics (right). Columns and rows of each panel represent the EMAC simulations (including the sensitivity experiments) and the given diagnostics (see Table 3), respectively. Where an alternative dataset is available, the diagram boxes are split in two parts, showing the model performance compared to the primary (lower triangle) and alternative (upper triangle) dataset. Where no observations are available, the triangles are marked white.

Title Page

Abstract Introduction

Conclusions References

Tables Figures

◀ ▶

◀ ▶

Back Close

Full Screen / Esc

Printer-friendly Version

Interactive Discussion

## Quantitative evaluation of ozone and selected climate parameters in EMAC

M. Righi et al.

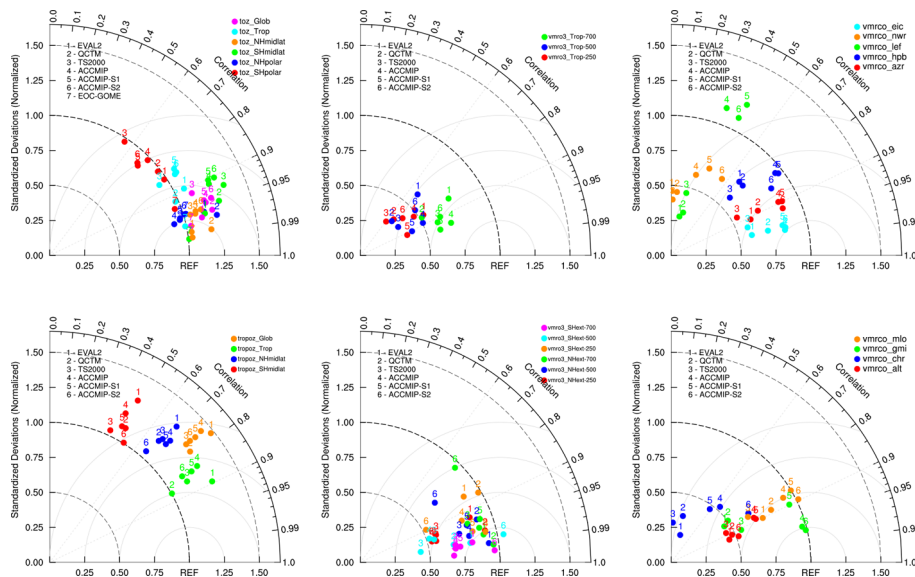


**Figure 12.** Taylor diagrams for total and tropospheric column ozone (left), ozone profiles (middle) and surface CO diagnostics (right).

Title Page

Abstract

Introduction

Conclusions

References

Tables

Figures

◀

▶

◀

▶

Back

Close

Full Screen / Esc

Printer-friendly Version

Interactive Discussion

## Quantitative evaluation of ozone and selected climate parameters in EMAC

M. Righi et al.

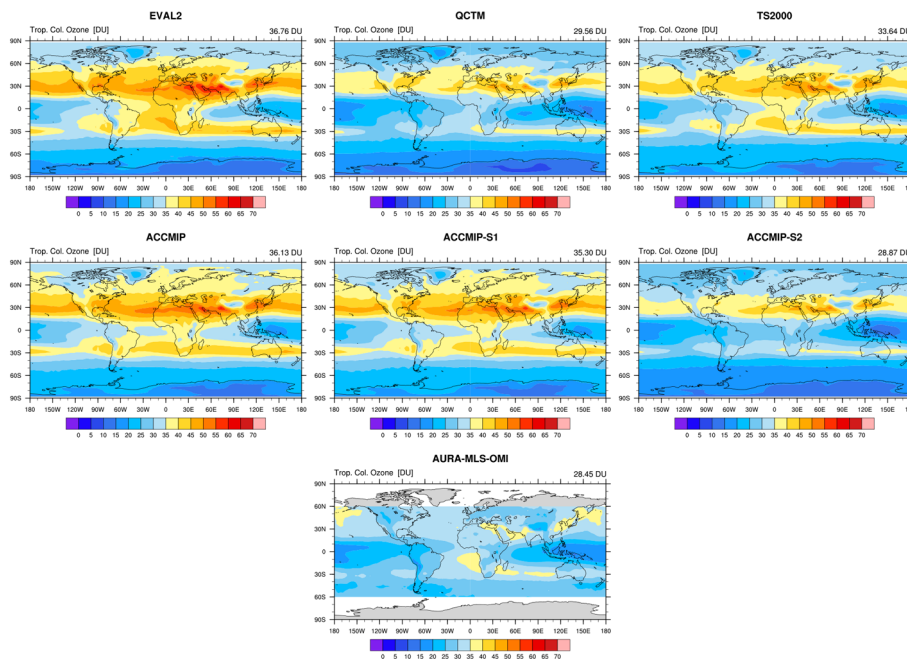


**Figure 13.** Tropospheric column ozone in the EMAC simulations compared to MLS/OMI observations. The values on top of each panel show the global (area-weighted) average, calculated after regridding the data to the horizontal grid of the model and ignoring the grid cells without available observational data.

Title Page

Abstract

Introduction

Conclusions

References

Tables

Figures

⏪

⏩

◀

▶

Back

Close

Full Screen / Esc

Printer-friendly Version

Interactive Discussion



## Quantitative evaluation of ozone and selected climate parameters in EMAC

M. Righi et al.

Title Page

Abstract

Introduction

Conclusions

References

Tables

Figures

◀

▶

◀

▶

Back

Close

Full Screen / Esc

Printer-friendly Version

Interactive Discussion

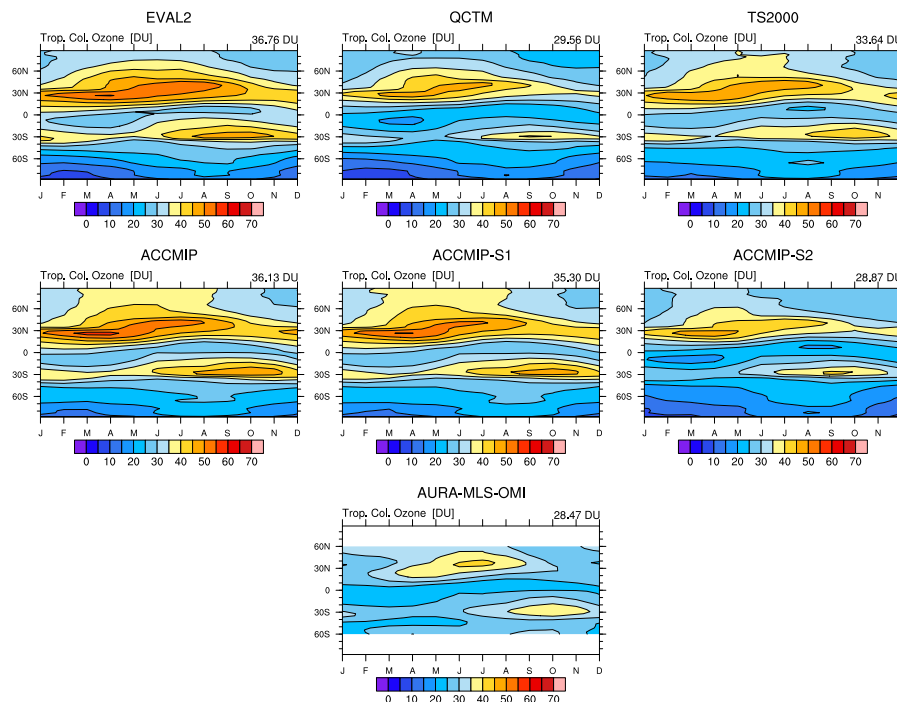


**Figure 14.** Annual cycle of the tropospheric column ozone climatology in the EMAC simulations compared to MLS/OMI observations. The values on top of each panel show the global (area-weighted) average, calculated after interpolating the observations on the model grid and ignoring the grid cells without available observational data.

## Quantitative evaluation of ozone and selected climate parameters in EMAC

M. Righi et al.

Title Page

Abstract

Introduction

Conclusions

References

Tables

Figures

◀

▶

◀

▶

Back

Close

Full Screen / Esc

Printer-friendly Version

Interactive Discussion

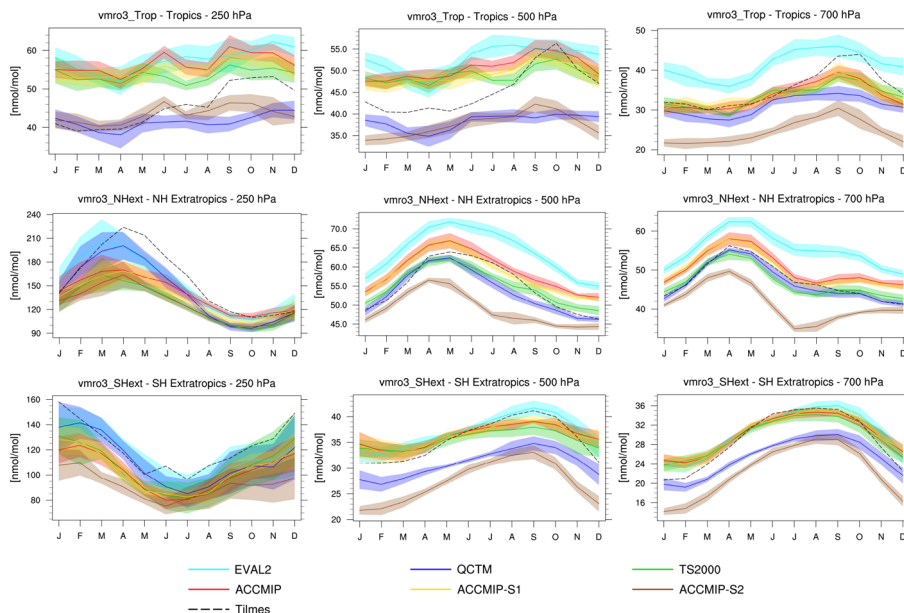


**Figure 15.** Annual cycle of ozone climatology in three regions (tropics, NH and SH extratropics) at three pressure levels (250, 500 and 700 hPa) for the EMAC simulations compared with ozonesondes data by Tilmes et al. (2012). Model and observational data are grouped into four latitude bands and sampled at three, with the models sampled at the ozonesonde locations before averaging together. The shaded areas indicate the  $\pm 1\sigma$  interannual variability (for EMAC only).



## Quantitative evaluation of ozone and selected climate parameters in EMAC

M. Righi et al.

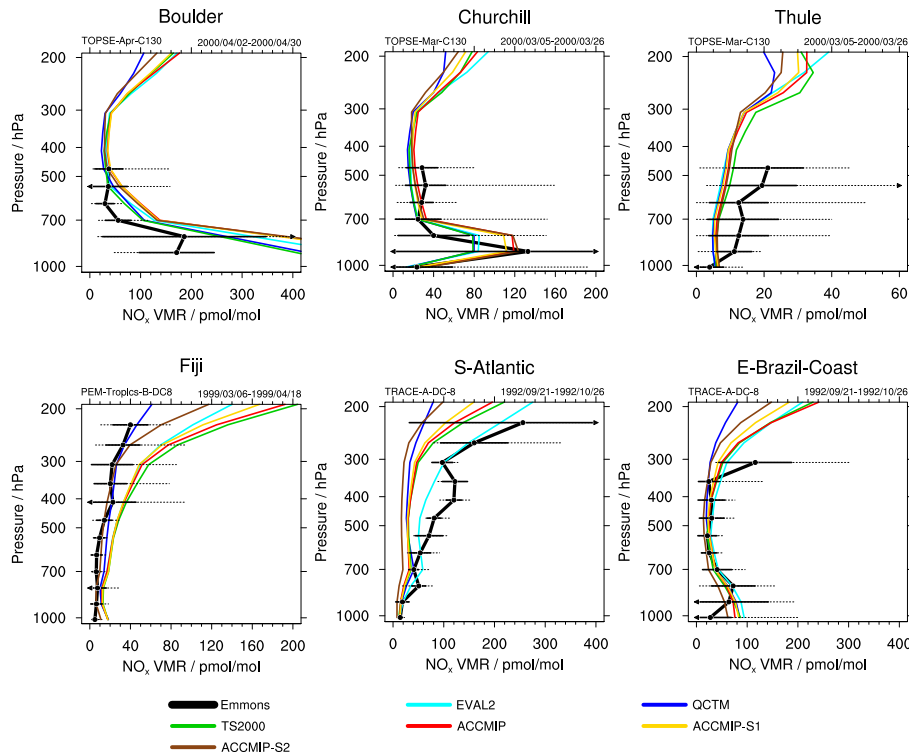


Figure 17. Similar to Fig. 16, for NO<sub>x</sub>.

[Title Page](#)  
[Abstract](#)   [Introduction](#)  
[Conclusions](#)   [References](#)  
[Tables](#)   [Figures](#)  
⏪   ⏩  
◀   ▶  
[Back](#)   [Close](#)  
[Full Screen / Esc](#)  
[Printer-friendly Version](#)  
[Interactive Discussion](#)





## Quantitative evaluation of ozone and selected climate parameters in EMAC

M. Righi et al.

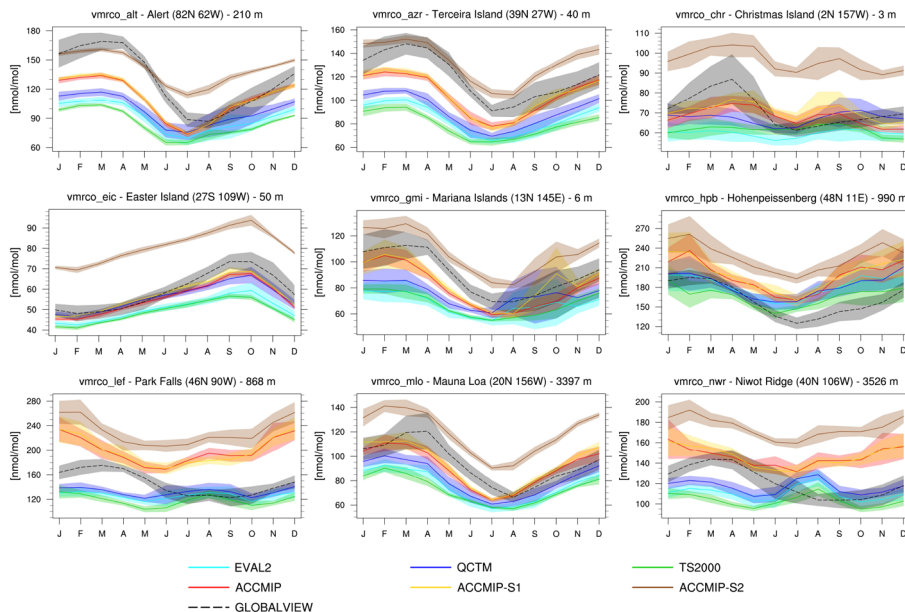


**Figure 19.** Annual cycle of CO surface concentration climatology for the EMAC simulations and NOAA GLOBALVIEW data, at nine different stations world wide. The shaded areas indicate the  $\pm 1\sigma$  interannual variability.

Title Page

Abstract

Introduction

Conclusions

References

Tables

Figures



Back

Close

Full Screen / Esc

Printer-friendly Version

Interactive Discussion

